INVESTIGATION OF THE EFFECTS OF BIOACTIVE PEPTIDE NANOFIBERS ON ACUTE MUSCLE INJURY REGENERATION

A THESIS SUBMITTED TO

MATERIALS SCIENCE AND NANOTECHNOLOGY PROGRAM

OF THE GRADUATE SCHOOL OF ENGINEERING AND SCIENCE

OF BILKENT UNIVERSITY

IN PARTIAL FULFILLMENT OF THE REQUIREMENTS

FOR THE DEGREE OF

MASTER OF SCIENCE

By

ÇAĞLA EREN ÇİMENCİ

October, 2016

INVESTIGATION OF THE EFFECTS OF BIOACTIVE PEPTIDE NANOFIBERS ON ACUTE MUSCLE INJURY REGENERATION

By Çağla Eren Çimenci,

October, 2016

We certify that we have read this thesis and that in our opinion it is fully adequate, in scope and in quality, as a thesis for the degree of Master of Science.

Ayşe Begüm Tekinay (Advisor)

Aykutlu Dana

Reyhan Neslihan Gürsoy

Approved for the Graduate School of Engineering and Science:

Ezhan Karaşan

Director of the Graduate School of Engineering and Science

ABSTRACT

INVESTIGATION OF THE EFFECTS

OF BIOACTIVE PEPTIDE NANOFIBERS ON

ACUTE MUSCLE INJURY REGENERATION

Çağla Eren Çimenci

MSc in Materials Science and Nanotechnology

Supervisor: Assist. Prof. Dr. Ayşe Begüm Tekinay, PhD

October, 2016

Skeletal muscle constitutes a large part of the human body. It is a hierarchically organized heterogeneous tissue and is composed of muscle fiber bundles, muscle fibers, myofibrils and myofilaments. Since muscle cells are terminally differentiated, they have limited capacity to renew themselves. Only new cells can fuse with muscle fibers and increase the size and volume of skeletal muscle. Myosatellite cells or satellite cells are small, mononuclear progenitor cells with virtually no cytoplasm. They are located in between the sarcolemma and basement membrane of terminally-differentiated muscle fibers. Satellite cells are precursors to skeletal muscle cells, and are able to give rise to satellite cells or differentiated skeletal muscle cells. They are normally found in silent state in adult muscle, but act as a reserve cell population that is able to proliferate in response to injury and give rise to regenerated muscle and to more satellite cells. Formation of the new muscular tissue is called myogenesis. During this event, satellite cells differentiate into myoblasts, and then myoblasts fuse with each other in order to form myofibers. There are many genes that regulate the myogenesis process and each of them is

activated in a different step of myogenesis. Increased or decreased levels of gene expression determine the differentiation capacity.

Peptide nanofibers are supramolecular structures formed via self-assembly and they are promising molecules in regenerative medicine and tissue engineering. Peptide-based molecules for tissue regeneration is a widely studied area and currently used in the treatment-investigation of many different tissues such as bone, cartilage, skin and nerve.

Since laminin is one of the most abundant proteins found in the basal membrane of the skeletal muscle; in this thesis, we designed and synthesized a laminin-mimetic bioactive (LM/E-PA) molecule functionalized with bioactive groups for mimicking laminin activities and capable of accelerating satellite cell activation. Our research group had previously shown that LM/E-PA containing nanofibers can support muscle differentiation *in vitro*. In this thesis, the clinical relevance was demonstrated further by assessing laminin-mimetic bioactive scaffold in acute muscle injury in an *in vivo* rat model. Our findings revealed that this scaffold system significantly promotes satellite cell activation in skeletal muscle and accelerates regeneration following acute muscle injury. In addition, our findings show that the regeneration capacity of the skeletal muscle was increased and consequently regeneration time was reduced. This study is one of the first examples of molecular level and tissue level regeneration of skeletal muscle by using bioactive peptide nanofibers following acute muscle injury, and shows that laminin mimetic nanofiber system is a promising material for development of new therapeutic curatives for acute skeletal muscle injuries.

Keywords: Skeletal muscle, acute muscle injury, peptide nanofibers, functional self-assembly, biomaterials, *in vivo*, rat model, laminin

ÖZET

BİYOAKTİF PEPTİT NANOFİBERLERİN AKUT KAS HASARI ÜZERİNDEKİ ETKİLERİNİN İNCELENMESİ

Çağla Eren Çimenci

Malzeme Bilimi ve Nanoteknoloji, Yüksek Lisans

Tez Danışmanı: Asist. Prof. Dr. Ayşe Begüm Tekinay

Ekim, 2016

İskelet kası insan vücudunun büyük bir kısmını kaplamaktadır. Hiyerarşik bir şekilde organize olmuş yapılardan meydana gelen heterojen bir dokudur. Bu hiyerarşik yapı, kas demetleri, kas fiberleri, miyofibriller ve miyofilamentlerden meydana gelmektedir. Kas hücreleri farklılaşmalarını tamamladıklarından dolayı kendilerini yenileme kapasiteleri oldukça kısıtlıdır. Kas yenilenmesi yalnızca yeni hücrelerin kas fiberleri ile birleşerek iskelet kasının boyutunu ve hacmini artırması ile gerçekleşmektedir. Kas uydu (satellit) hücreleri küçük ve tek çekirdek içeren kas öncül hücreleridir ve neredeyse hiç sitoplazmaları yoktur. Sarkolemma ve kas fiberlerinin bazal membranı arasında yer alırlar. Satellit hücreler iskelet kası öncül hücreleridir ve gerektiğinde kasa farklılaşabildikleri gibi satellit hücre havuzunu korumak için asimetrik bölünme ile satellit hücre olarak da kalabilirler. Normalde sessiz durumda beklerler fakat bir hasar durumu söz konusu olduğunda aktifleşip farklılaşmaya başlarlar. Yeni kas dokusu oluşturulması işlemine miyogenez adı verilir. Bu olay sırasında, satellit hücreler miyoblastlara farklılaşır ve miyoblastlar biraraya gelerek miyofiberleri meydana getirir. Miyogenezi

düzenleyen birçok gen vardır ve bu genlerden her biri miyogenezin farklı bir aşamasında aktifleşmektedir. Genlerin artması ve azalması ile hücrelerin farklılaşma kapasiteleri belirlenmektedir.

Peptit nanofiberler kendiliğinden biraraya gelerek oluşan çok moleküllü yapılardır ve rejeneratif tıp/doku mühendisliği alanında gelecek vaat eden moleküllerdir. Doku mühendisliğinde peptit tabanlı moleküllerin kullanılması geniş bir çalışma alanıdır ve kemik, kıkırdak, cilt ve sinir gibi birçok dokunun tedavi araştırmalarında kullanılmaktadır.

İskelet kasında en fazla bulunan moleküllerden biri olması sebebi ile bu tez çalışmasında laminini taklit eden peptit molekülleri (LM/E-PA) tasarlanıp sentezlenmiştir. Biyoaktif grubu laminin molekülünü taklit edecek şekilde işlevsel hale getirilmiştir ve bu grup satellit hücre farklılaşmasını hızlandırmaktadır. Daha önce grubumuzda yapılmış olan bir çalışma da LM/E-PA molekülünün hücresel düzeyde kas farklılaşmasına destek olduğu gösterilmiştir. Bu tez çalışmasında ise araştırmalar bir adım ileriye taşınarak malzemenin klinik önemi *in vivo* sıçan modeli üzerinde araştırılmıştır. Bulgularımız iskelet kasının yenilenme kapasitesinin arttığını ve buna bağlı olarak yenilenme süresinin kısaldığını göstermektedir. Bu çalışma, biyoaktif peptit nanofiberlerin akut kas hasarı üzerindeki doku ve molekül seviyesindeki iyileşmeye etkilerinin araştırıldığı ilk çalışmalardan biridir. Özet olarak, laminini taklit eden biyoaktif iskele sistemleri kas hasarına karşı yeni tedavi yöntemlerinin geliştirilmesinde gelecek vaat eden malzemelerdir.

Anahtar kelimeler: İskelet kası, akut kas hasarı, peptit nanofiberler, işlevsel supramoleküler nanoyapılar, biyomalzemeler, *in vivo*, sıçan modeli, laminin

ACKNOWLEDGEMENTS

It would not have been possible to write this thesis without to help and support of the kind people around me. First, I would like to express my sincere appreciation and gratitude to my advisors, Prof. Ayşe Begüm Tekinay and Prof. Mustafa Özgür Güler for their guidance and support to my research. I'm grateful for their patience, motivation and immense knowledge helped me develop a trans-disciplinary research skills, which I can carry with me throughout my research career.

I would like to acknowledge the graduate scholarship from TÜBİTAK (The Scientific and Research Council of Turkey) BIDEB 2210-C for financial support.

I also would like to thank Gözde UZUNALLI for her helpful suggestions and comments during my first year study, Elif ARSLAN for her patience, encouragement and precious answers for my endless questions. I would like to express my special thanks to Özge UYSAL for her diligence and assistance while I was working in the lab.

I also would like to thank other "cartilage subgroup" members; Özüm Şehnaz ÇALIŞKAN, Nurcan HAŞTAR and İbrahim ÇELİK for creating such a warm working environment with their team spirit and friendship.

Special thanks to Melike SEVER (one of the reason why I'm here) for teaching me the survival methods in graduate life and her excellent friendship. If I had a chance, I would like to carry Seren HAMSİCİ everywhere with me, I appreciated for her true friendship.

Thanks to the current and former members of Nanobiotechnology and Biomimetic Materials laboratory group at the UNAM. I would like to wish the best for their graduate journey to Zeynep ORHAN, Gökhan GÜNAY, İdil UYAN, Canelif YILMAZ, Gülistan TANSIK, Mustafa

BETER, Merve ŞEN, Fatih YERGÖZ, Nuray GÜNDÜZ, Ahmet Emin TOPAL, Oğuz TUNCAY and Burak DEMİRCAN who became my family and they have made my graduate life unforgettable.

I would like to acknowledge Dr. Ebru UMAY and Dr. Ece ÜNLÜ who believe in my project and helped me for electromyographical analysis in animal studies. I also would like to thank to Alper Devrim ÖZKAN for his fruitful comments and proofread.

Moreover, I would like to express my most sincere thanks to my roommate Behide SALTEPE for making my home life spirited and peaceful. She was always with me when I wanted to talk and we shared so many things that two people can share. A very special thank you to my friends Recep Erden AHAN and Onur APAYDIN for the cheer and support you have lent me over all my graduate life. I had chance to know better Tuğçe ÖNÜR in Ankara, she was always ready for every kind of outdoor activities with me and deserves all compliments with her friendship.

Moreover, I would like to thank to my beloved sister Başak EREN who is not just a sister but also my best friend. She is the best architect I've ever known, helped me a lot with her advanced photoshop skills. My little brother Can EREN who was always cheering me up with his sense of humor. Also, my father Cahit EREN and my mother Şükran EREN who always encouraged me and helped me became who I am. I am grateful for their patience and sacrifice that will remain my inspiration throughout my life. I am also very much grateful to all my family members for their constant inspiration, unconditional confidence and love. Their positive outlook on life has given me the strength to do it all.

Finally, I want to thank to my husband Kadir ÇİMENCİ who makes me feel motivated, who was always supporting and encouraging me when I encounter difficulties. His continued and unfailing love helped me to keep dreaming and deserves all compliments.

Last, but not least, I send big thanks to all my friends from İstanbul, who always support me, give me good advices and make my life colorful!

I love you with all my heart.

Çağla

CONTENTS

LIST OF FIGURES

LIST OF TABLES

ABBREVIATIONS

BCA : Bicinchoninic acid

BSA : Bovine serum albumin

β-gal : β-galactosidase

CD : Circular dichroism

CD34 : Hematopoietic progenitor cell antigen CD34

Col-I : Collagen type I

Col-III : Collagen type III

DCM : Dichloromethane

DMF : N, N-Dimethylformamide

DMEM : Dulbecco's modified Eagle's medium

DMSO : Dimethylsulfoxide

ECL : Enhanced chemiluminescence

ECM : Extracellular matrix

EDTA : Ethylenediaminetetraacetic acid

EGF : Epidermal growth factor

EMG : Electromyography

FBS : Fetal bovine serum

FDA : U.S. Food and Drug Administration

bFGF : Basic fibroblast growth factor

GAG : Glycosaminoglycan

GAPDH : Glyceraldehyde 3-phosphate dehydrogenase

GF : Growth factor

H&E : Hematoxyline & eosin staining

HGF : Hepatocyte growth factor

HUVEC : Human umbilical vein endothelial cell

HPLC : High performance liquid chromatography

HRP : Horseradish peroxidase

IGF : Insulin like growth factor

IgG : Immunoglobulin G

kDa : Kilo dalton

LC-MS : Liquid chromatography-mass spectrometry

LM/E-PA : Laminin mimetic bioactive peptide amphiphile

MLC3F-tg : Myosin light chain 3F transgenes

MRFs : Myogenic regulatory factors

Myf5 : Myogenic factor 5

MyoD1 : Myogenic differentiation 1

NSAIDs : Non-steroidal anti-inflammatory drugs

IHC : Immunohistochemistry

PA : Peptide amphiphiles

Pax7 : Paired box 7

PBS : Phosphate-buffered saline

PCR : Polymerase chain reaction

Q-TOF : Quadrupole time of flight

RICE : Rest, ice, compression, elevation

RIPA Buffer : Radioimmunoprecipitation assay buffer

RT-qPCR : Reverse transcriptase quantitative polymerase chain reaction

SC : Satellite cell

SDS : Sodium dodecyl sulfate

SDS-PAGE : Sodium dodecyl sulfate-polyacrylamide gel electrophoresis

SEM (M) : Scanning electron microscope

SEM (S) : Standard error of the mean

STEM : Scanning transmission electron microscope

TA : Tibialis anterior

TBS : Tris-buffered saline

TBS-T : Tris-buffered saline-Tween 20

TIS : Triisopropylsilane

TCP : Tissue culture plate

TEM : Transmission electron microscope

TEMED : Tetramethylethylenediamine

TFA : Trifluoroacetic acid

TGF-β1 : Transforming growth factor beta 1

VEGF : Vascular endothelial growth factor

WHO : World Health Organization

Investigation of the Effects of Bioactive Peptide Nanofibers on Acute Muscle Injury Regeneration

This work is partially described in the following publication:

Cagla Eren Cimenci *, †, Gozde Uzunalli *, †, Ozge Uysal *, †, Fatih Yergoz *, †, Ebru Karaca Umay ‡, Mustafa O. Guler *, †, §, Ayse B. Tekinay *, †, §

(Manuscript under Submission)

1. Objective

While the causes of muscle injury are numerous and diverse, acute injuries caused by excess pressure, shocks, falls and crushing damage are among the most widespread. Sports, heavy lifting and other strength-intensive tasks are both ubiquitous in modern life and likely to cause acute skeletal muscle injury. Even though skeletal muscle exhibits the capacity for self-renewal, this regeneration may take months. As such, speeding up the regeneration of skeletal muscle injuries would not only shorten the duration of recovery for the patient, but also support the general health and functionality of the repaired muscle tissue. In this work, we designed and synthesized a laminin-mimetic PA molecule that is functionalized with bioactive groups for mimicking laminin activities. We then created an acute tibialis anterior muscle injury in a rat model and injected the PA hydrogel to the injury site. Peptide amphiphile hydrogels are ideal scaffold systems for regenerative medicine studies due to their ease of injection. Following the local administration of PA scaffolds, we evaluated the regeneration and differentiation capacity of skeletal muscle through behavioral, histological/physiological

and molecular analyses. Our results suggest that the laminin-mimetic biomaterial system assists skeletal muscle regeneration and that peptide nanofibers are highly promising for the regeneration of acute muscle injuries. This work demonstrates for the first time that laminin-mimetic self-assembled peptide nanofiber networks facilitate myogenic differentiation *in vivo* without the need for additional treatment.

2. Introduction: Skeletal Muscle Tissue Engineering

2.1. Muscle Tissue

Skeletal muscle constitutes a great proportion of the vertebrate body. It provides postural support and facilitates the movements of the body through its contractions. Skeletal muscle is the most common muscle type among the three varieties of muscle. It has a hierarchical fiber organization (Figure 1) that encompasses multinucleated and parallel-aligned muscle fibers in each muscle.

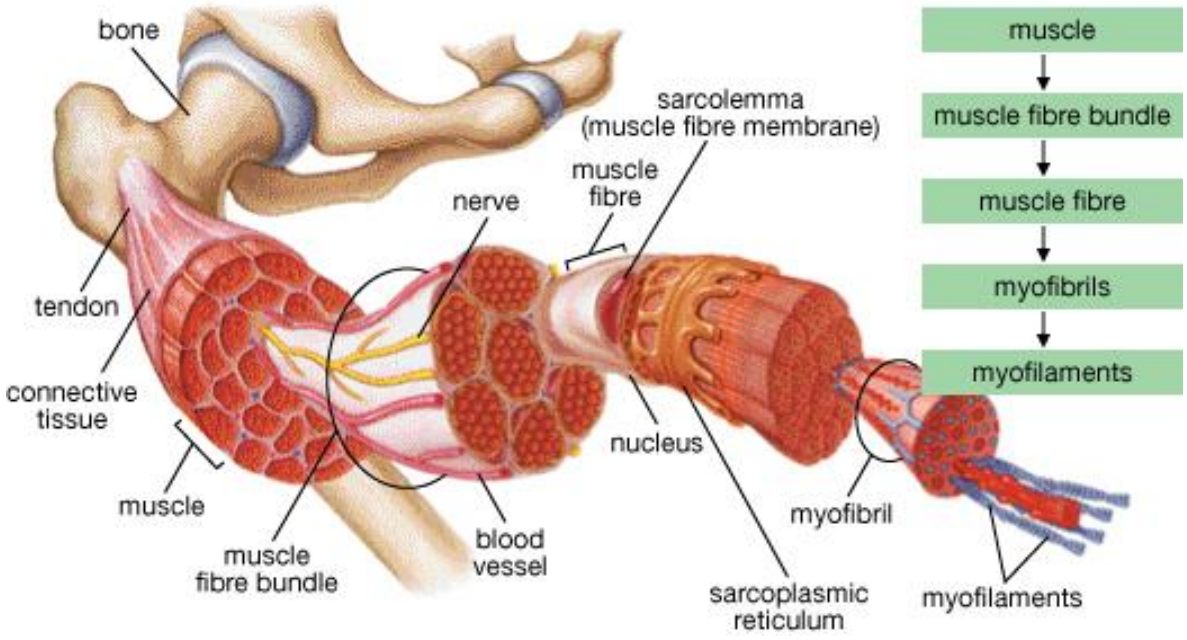

Figure 1 Schematic illustration of the hierarchical organization of skeletal muscle. Adapted from Helene Colbourne et al, Inquiry into Biology (Toronto: McGraw-Hill Ryerson, 2007), p. 335.

In contrast to smooth muscle and cardiac muscle, skeletal muscle provides and controls intentional body movements. It is similar in shape to the myocardium; however, skeletal muscle has multinucleated, thin and long fibers. Nerves and blood vessels assist the skeletal muscle and provide communication between individual fibers, while connective tissue facilitates the attachment of these fibers to each other[1]. Muscle fibers are affected by several types of physical activity and status; including exercise, physical injury, disease and aging. Skeletal muscle has remarkably high adaptive capacity and readily alters its size and shape in response to external stimuli[2]. Correct measurement of muscle mass is an important parameter because it is strongly and directly related with the skeletal muscle strength[3].

2.2. Problems Related with Muscle Tissue

Skeletal muscle tissue is susceptible to damage following exposure to excess pressure, shocks, drops, crushing damage, exercise, and sports injuries. Consequently; sports, heavy lifting and high performance-tasks are likely to cause acute skeletal muscle injury. Acute muscle injuries arise suddenly and cause severe and painful strains. Skeletal muscle damage is among the most frequent sports- and exercise-related injuries[4]. Its treatment is very limited and mostly ameliorative, often focusing on the mitigation of local pain and swelling. Long-term muscle problems may occur in 10% to 55% of all muscle injuries[5].

Besides being adapted to environmental changes, skeletal muscle presents a spectacular regeneration capacity in response to small injuries[6]. In such cases, restoration of the slightly damaged muscle is possible without any therapeutic intervention[7]. However; if

damage is severe and left untreated, it may lead to loss of muscle mass and function. In these cases, skeletal muscle regeneration cannot be completely facilitated by the help of medical treatment or surgical reconstruction[8]. Accordingly, improving effective treatment methods against major skeletal muscle injuries is a growing area of interest[9]. Novel methods have been developed to support the recovery of heavy muscle injuries, often with spectacular results.

Skeletal muscle injury diagnosis is primarily performed by checking the history of the injury and using this as a guideline to determine the requisite set of clinical investigations. Non-invasive imaging is another helpful technique for the detection of muscle mass loss, and allows one to make accurate predictions about the prognosis of the injury[10]. The optimal therapeutic method can be determined for each individual case through the use of these approaches.

Muscular abnormalities can also arise as a result of problems with the nervous system, genetic mutations, malnutrition, and abuse or straining of muscles. Muscular dystrophy is caused by abnormal neurological signals and presents through the degeneration or abnormal development of muscular fibers[11]. Muscular hypertrophy involves the aberrant increase of muscle mass and may result from repeated, minor skeletal muscle damage, often as a consequence of physically demanding work. In this case, muscle cells grow continuously to compensate for the muscle damage, creating an increase in fiber diameters and overall muscle mass[12]. Muscular atrophy describes misused or unused muscles that shrink because of the lack of neurological connections, resulting in a degenerate morphology and decreased muscle mass[13]. Muscle injuries related to the nervous system, genetic mutations and malnutrition are long-term problems arising from

indirect causes. However, our main focus in this project is acute muscle injuries (which are caused by traumas) and their treatments. These type of injuries occur by the effect of *direct causes* such as crushing pressure, excess work, shocks, fall injuries etc.

2.3. Muscle Tissue Repair

Satellite cells are considered to be skeletal muscle progenitor cells and are found in between the basal lamina and the plasma membrane (Figure 2). They promote the growth, repair and regeneration of skeletal muscle fibers[14]. They are unipotent cells and have self-renewal capacity.

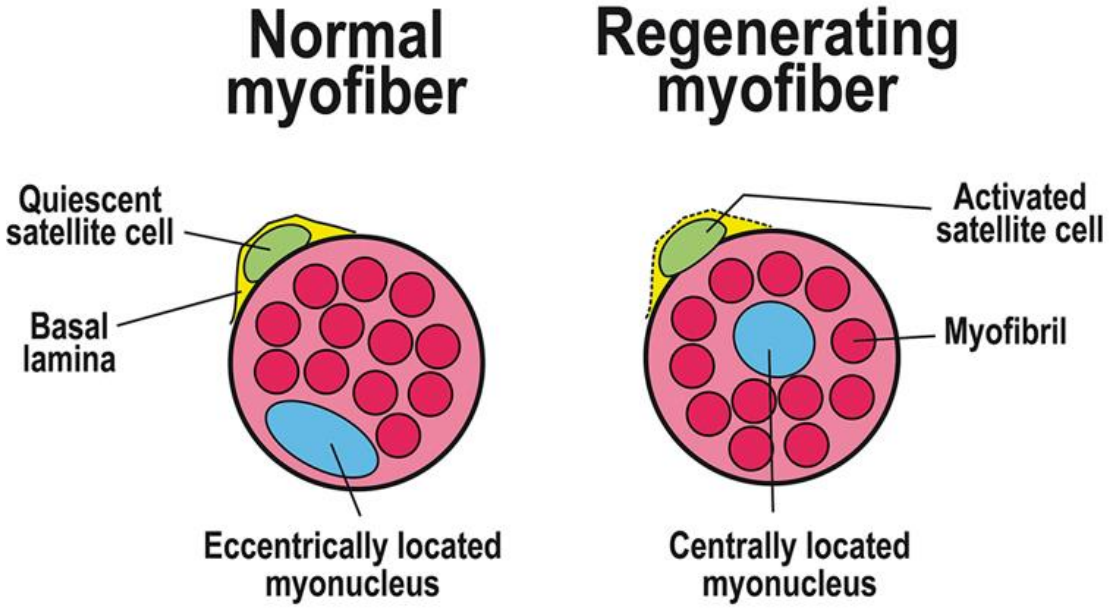

Figure 2 Localization of satellite cells (muscle progenitors) into the skeletal muscle fibers[16]. In normal myofibers, quiescent satellite cells are found in between the plasma membrane and the basal lamina. However in regenerating myofibers, activated satellite cells merge with the fiber and are localized at the center of the muscle fibers.

Through these characteristics, satellite cells maintain their existence within the muscle while protecting the self-repair ability of muscle after damage. When skeletal muscle is damaged, satellite cell activation takes place and muscle regeneration occurs through four main stages; degeneration, inflammation, regeneration and remodeling[15]. Following injury, activated satellite cells initially merge with muscle fibers and are localized at their centers. As such, centrally located nuclei are often observed within newly regenerated fibers and this situation is a strong indicator of active muscle regeneration.

Myogenesis is the process of muscle development. New muscle fibers are formed through the fusion of satellite cells with the existing fibers; which are multinucleated, post-mitotic and highly differentiated[17]. Sequentially ordered events constitute the skeletal muscle regeneration process (Figure 3). The first step of myogenesis is the **degeneration** step, where the integrity of skeletal muscle is disrupted because of trauma. Basal lamina and sarcolemma are demolished and the fibers are exposed to extracellular calcium, which results in their rupture and destruction[18].

Degeneration is followed by the **inflammation** step, which is an early response to degeneration and provides a connection between the site of injury and the immune system. Activated macrophages and neutrophils are then recruited and tissue debris is removed.

Pro-inflammatory and anti-inflammatory cytokines are produced by these cells, resulting in the activation of satellite cells and leading to the **regeneration** phase[19]. In muscle tissue, regeneration begins at the first week (approximately 4^{th} and 5^{th} day) after injury[20]. After satellite cells are completely activated, stem cells are recruited and muscle fibers

start to regenerate. Myoblasts also proliferate and differentiate at this step, which culminates in their fusion into myofibers and the formation of mature myofibers[21]. Growth factors like IGF-1, bFGF, EGF, HGF and TGF-β1 are known to play vital roles in the regeneration step[22].

Overlapping with regeneration is the **remodeling** phase, which is the fourth step of skeletal muscle regeneration and entails the remodeling of the extracellular matrix, which is very crucial for muscle integrity. This phase starts at day 7-10 and lasts up to 14-28 days, depending on the injury. VEGF is also secreted at this phase and triggers local angiogenesis in the regenerating skeletal muscle. This leads to the formation of an extensive capillary network and allows the effective delivery of O_2, nutrients and growth factors to newly formed muscle fibers[23].

The last and the longest phase of the skeletal muscle regeneration is **maturation**. Skeletal muscle gains its functional ability in this phase, but this phase can last up to 3 or 6 months depending on the injury[24]. Neurological connections are established completely and intramuscular nerve branches reach to the muscle fibers in the maturation step.

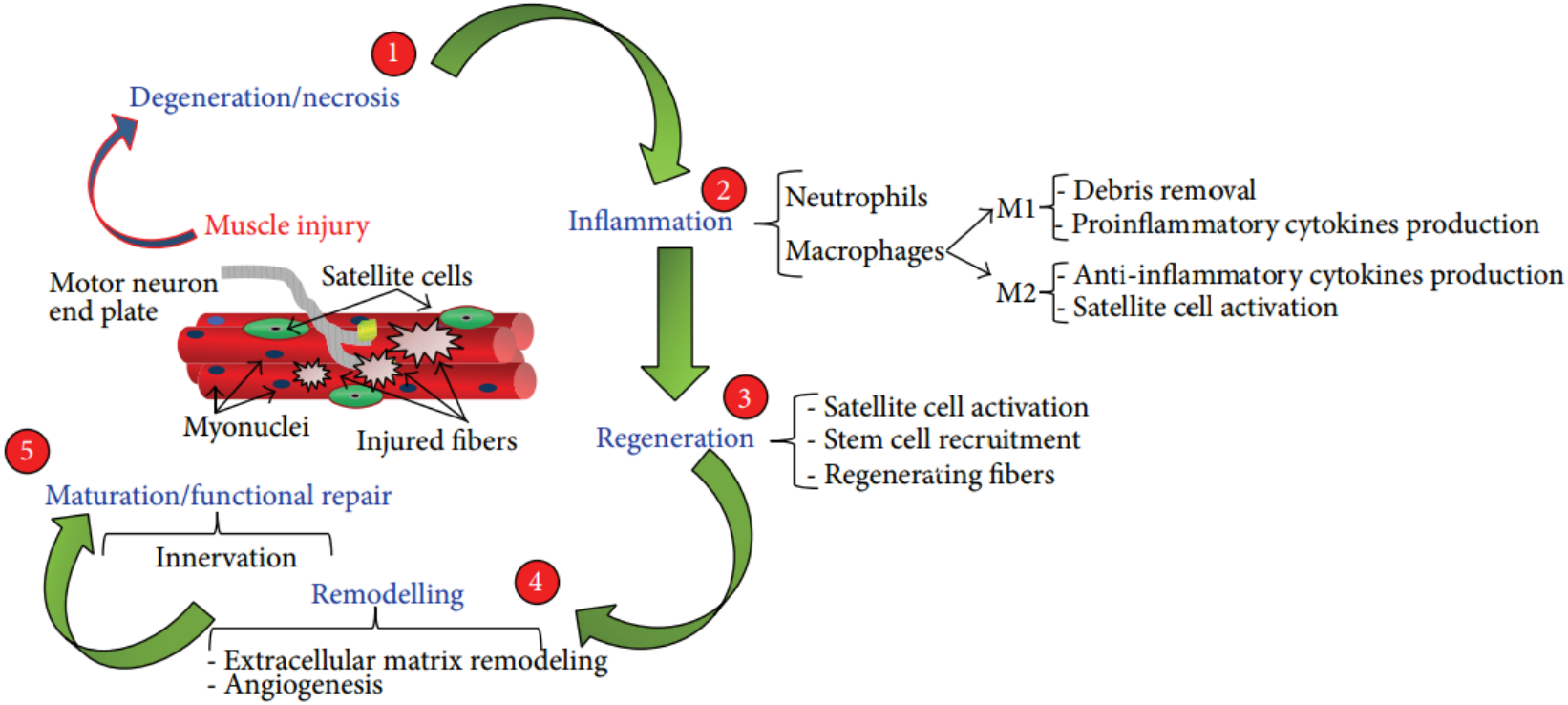

Figure 3 Schematic representation of the steps involved in skeletal muscle regeneration: Degeneration, Inflammation, regeneration, remodelling and maturation (Musarò et al., 2014).

Each regeneration step of the skeletal muscle actually overlaps with both the previous step and the following step (Figure 4). Such fusion is triggered by the temporally ordered changing of gene expression profiles of the myoblast cells, which allows the formation, maturation and differentiation of myotubes[25].

Pax7 is a transcription factor and expressed from quiescent satellite cells. Activation of satellite cells leads to Pax7 expression, which in turn mediates the maintenance of satellite cells. As seen in Figure 5, satellite cells undergo asymmetric division. One cell differentiates into a myocyte, while the other remains as a satellite cell in order to conserve the satellite cell pool[26].

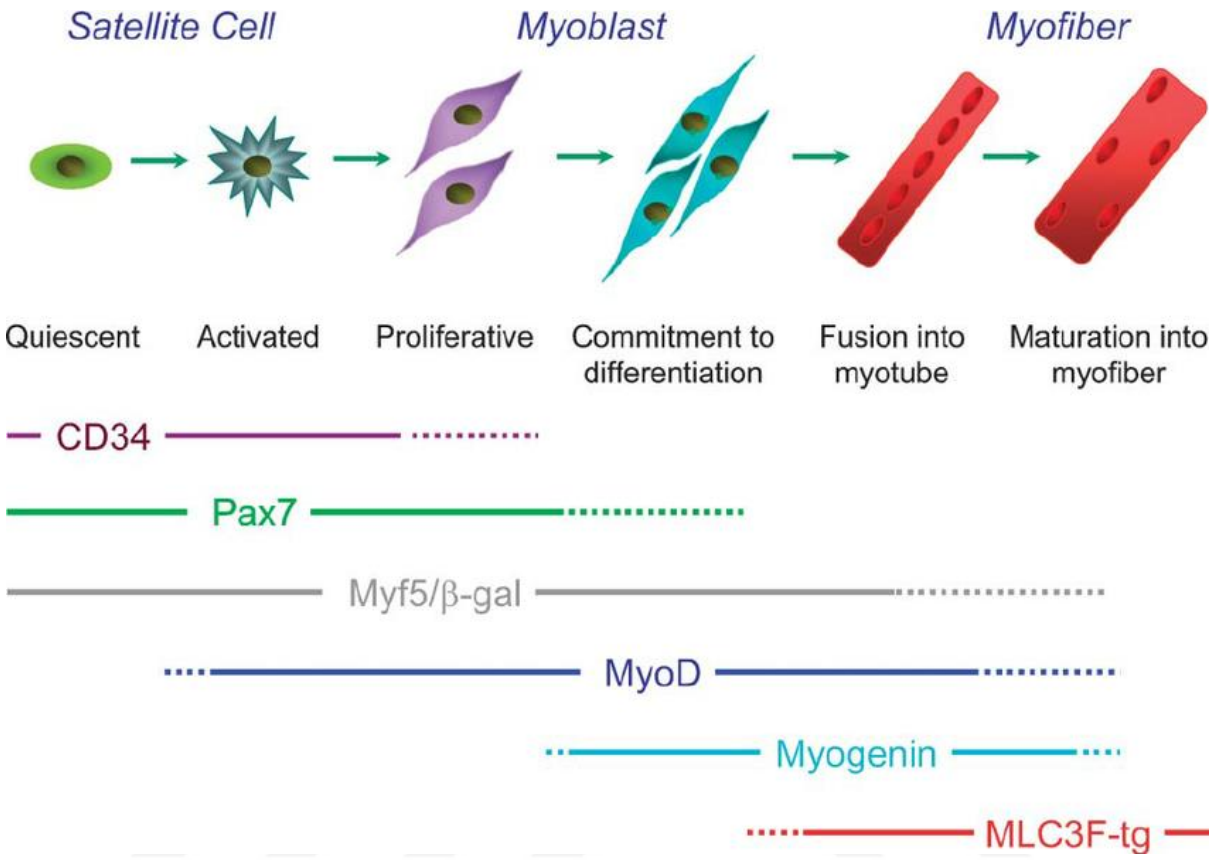

Figure 4 Schematic representation of muscle myogenesis and myogenesis markers. Specific markers for each step are illustrated in the order of their expression.

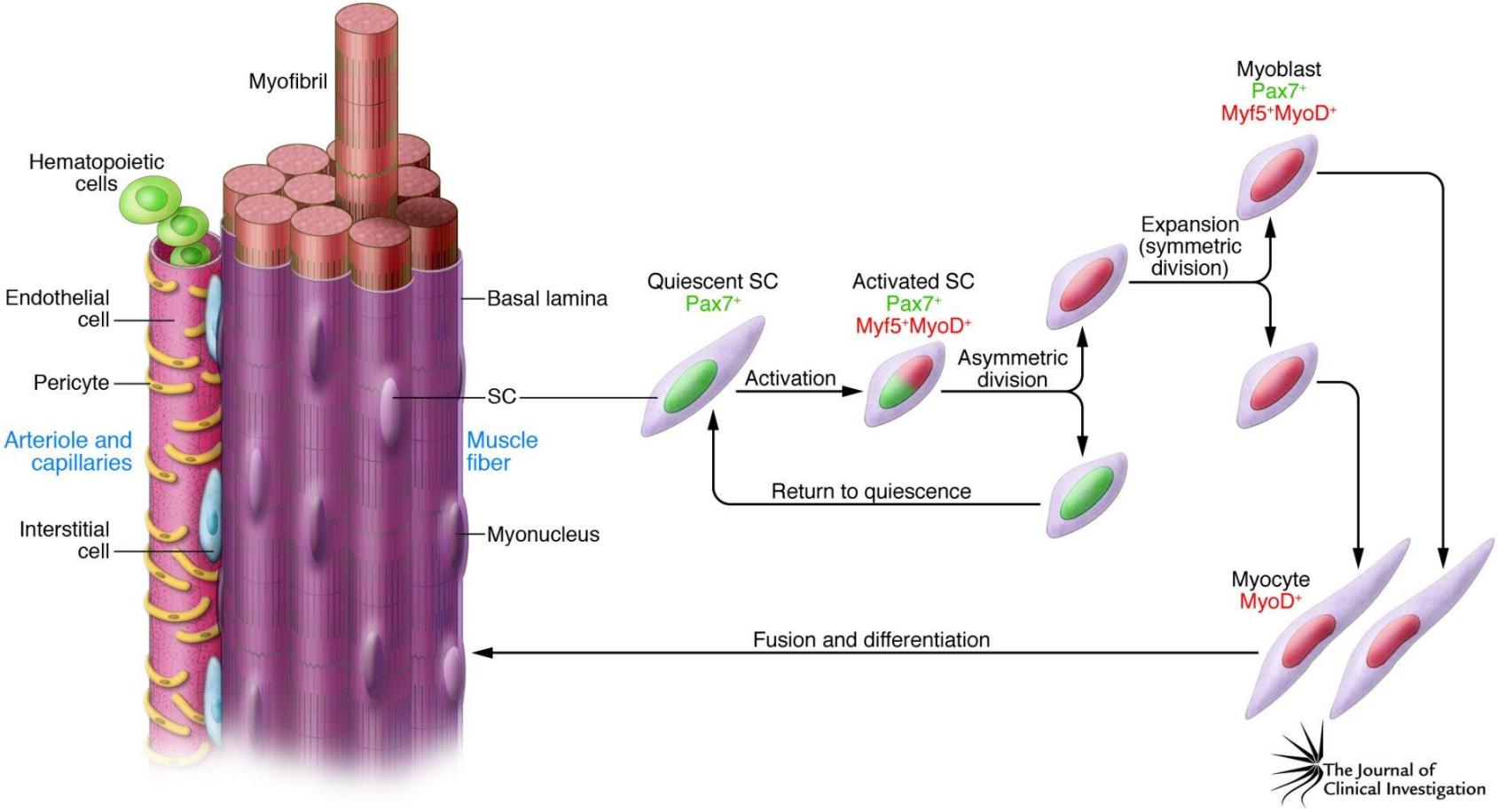

Figure 5 Schematic Illustration of the Asymmetric Division of Satellite Cells.

Myf5 is another transcription factor that is responsible for the activation of satellite cells during myogenesis. Myf5 is one of the earliest markers for myogenesis and it is a member of the myogenic regulatory factor family (MRFs). About 10% of Pax7+ satellite cells do not express Myf5; these cells are attached to the basal lamina at all times (even during SC proliferation) and considered to be *stem cells* for muscle tissue. Cells that express both Myf5 and Pax7, in contrast, are considered to be *muscle progenitor cells* and are more prone to differentiation[27].

MyoD1 is also a member of the myogenic regulatory factor family (MRFs). MyoD is activated as a result of exercise or damage, and triggers satellite cell activation. It is known that the combination of MyoD and Myf5 is extremely necessary for skeletal muscle myogenesis[28]. Another study shows that satellite cells have different fates according to the expression balance between Pax7 and MyoD. Pax7+ / MyoD– cells return to quiescent satellite state while Pax7+ / MyoD+ cells are committed to myogenic differentiation[29].

Myogenin is a transcription factor and also known as myogenic factor 4. It is one of the latest markers of skeletal muscle regeneration and essential for functional muscle formation. Myogenin controls the formation of myocytes from myoblasts and regulates terminal differentiation; consequently, this marker is upregulated in myogenesis[30].

2.4. Skeletal Muscle Proteins

Skeletal muscle is characterized by well-defined bands that are composed of thick and thin filaments. Such filaments constitute a series of arranged structures called *sarcomeres*. Sarcomeres are protein-based architectures and those proteins are divided

into two main subgroups; structural & functional and extracellular proteins. Accordingly, some sarcomeric proteins are intracellular, while others are secreted to the extracellular matrix to perform their functions.

2.4.1. Structural and Functional Proteins

They are mainly responsible for controlling the shape and function of the skeletal muscle. Muscle fibers are the smallest functional units of muscle, and their main function is to contract. Actin, myosin, troponin, tropomyosin and titin are the main proteins that are vital for muscular shape and function[31].

2.4.1.1. Actin

Actin is a major element of the *thin filaments*, which work in conjunction with myosin and provide contractile movements through the "sliding" of each protein over its neighboring component. This facilitates the contraction or shrinking of the actin filaments, which is translated to muscle movement[32].

2.4.1.2. Myosin

Myosin is another structural protein and, together with the actin, is the most abundant protein found in the structure of skeletal muscle. Myosin is a major element of the *thick filaments*, where one myosin molecule is bound from its end to other independent myosins and creates cross bridge[33].

2.4.1.3. Troponin

Troponin is a Ca^{+2}-binding protein that plays an important role in muscle contraction. Tropomyosin and actin both interact with troponin, and their relative affinity to this protein determines the behavior of the muscle fiber. Troponin ordinarily prevents the attachment of cross bridges and stops contraction in the relaxed muscle. If calcium channels open by the effect of stimulation, the incoming calcium ions bind to troponin. This causes a change in the conformation of troponin, resulting in a corresponding change in actin and myosin filaments and the contraction of the muscle fiber[34].

2.4.1.4. Tropomyosin

Tropomyosin movement is led by Ca^{+2}-bound troponin, which changes its conformation to facilitate the contraction process. This exposes the actin-affine site of tropomyosin, allowing it to interfere with actin-myosin interactions and mediate muscle contraction[35].

2.4.1.5. Titin

Titin is a structural protein that is responsible for stabilizing myosin filaments, so that they remain in the middle of the z-lines in the skeletal muscle. When contraction ends, it allows the muscle fibers to return to the resting state. In short, mechanical characteristics of the muscle are determined by titin[36].

2.4.2. ECM Proteins

Skeletal muscle extracellular matrix (ECM) is composed of a variety of proteoglycans and proteins that support muscle structure, provide cellular aggregation and create a suitable environment for cell migration[37]. Apart from these direct effects, the ECM can

also affect muscle cells indirectly by mediating binding interactions between growth factors and their receptors. As such, cellular communication occurs largely through muscle ECM[38]. Glycoproteins and polysaccharides are the main constituents of the ECM of the skeletal muscle and their assembly creates a macro-structured fiber architecture. Laminin, collagen, fibronectin and tenascins are protein-based components of the skeletal muscle, while glycosaminoglycans and proteoglycans are the main polysaccharides of the muscle ECM[37]. For this thesis project, I focused on the laminin protein, but information on collagen is also provided on account of its profound importance for the muscle extracellular matrix.

2.4.2.1. Collagen

Collagen IV is one of the main extracellular matrix components of skeletal muscle, and interacts with laminin (Figure 6) to form sheet-shaped networks that provide skeletal muscle with most of its elastic properties[39]. Collagen IV and laminin can therefore be regarded as the main building blocks of the muscle ECM. In addition to collagen IV, collagen I also covers the outer layer of the muscle fibers[40].

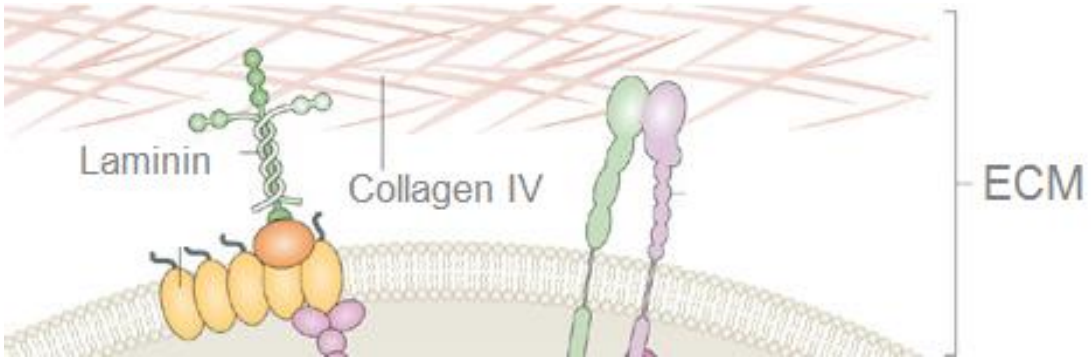

Figure 6 Schematic illustration of the interaction between laminin and type IV collagen in the ECM of the skeletal muscle.

2.4.2.2. Laminin

Laminin is one of the best-studied ECM proteins and can occur in several different forms. Laminin has α, β and γ chains that are arranged in a distinctive cross shape. As muscle basal membranes are rich in laminin and formed very early in embryonic development[41], this protein can be tracked to follow the formation of skeletal muscle. Laminin is also one of the major ECM elements in skeletal muscle tissue and binds directly to the collagen IV[42]. Laminins constitute a group of glycoproteins that are present in all basement membranes and play a role in the protection of muscle fibers from damage, as well as in the regeneration of the skeletal muscle[43].

The natural environment of satellite cells contains inducers of myogenic differentiation and muscle fiber development, and its emulation is a vital aspect of successful muscle injury treatment methods. It was previously proven that laminin has a crucial role in myogenesis and triggers the fusion of satellite cells, resulting in higher proliferation and skeletal muscle repair[44 45]. The IKVAV peptide sequence is derived from the β1 and α1 cell-binding domains of laminin and has been utilized to mimic the natural extracellular environment of skeletal muscle tissue[46].

2.5. Artificial Muscle

Although the concept of the artificial muscle is exciting, its current implementation leaves much to be desired. Both polymer and electronic artificial muscles are still substantially slower compared to biological muscles. Intentional movements have not been elicited in these muscles, and contractions over 60% are not possible without permanent damage. Furthermore, regeneration is impossible in current artificial muscle

systems: While synthetic materials capable of replicating the functions of muscle are promising for the treatment of muscle injuries[47], no self-repairing artificial muscle system has been described to date.

2.6. Other Treatment Methods

RICE (rest, ice, compression and elevation) is the traditional treatment method for muscle damage, and focuses on the alleviation of pain and secondary symptoms. Physical therapy and NSAIDs (non-steroidal anti-inflammatory drugs) are also recommended for the treatment of skeletal muscle injures[48]. No consensus exists on whether these treatments are truly effective.

The administration of growth factors (GFs) is a more promising approach for supporting the total functional regeneration of muscle tissue, as GFs have been suggested to control the progenitor cell differentiation and myotube formation from satellite cells. TGF-β1, for example, has been shown to be inhibited by the effect of TGF-β1 antagonists, which prevent skeletal muscle fibrosis by blocking the accumulation of collagen[49].

Antioxidant treatment was also shown to improve the regeneration of skeletal muscle[50]. One disadvantage of this method is that treatment has to be continued for 6 months, which is a considerably lengthy recuperation period for muscle injuries.

2.7. Clinical Significance of Biomaterials

Recent developments in biomaterial fabrication methods have allowed the design and production of novel materials for the regeneration of skeletal muscle[14]. Tissue engineering scaffolds are designed to bear physiochemical and biological characteristics

similar to the tissues they are intended to supplement. As such, both natural and synthetic biomaterials have been used to mimic the architectural and biomechanical features of various tissue types[51]. Peptides are promising materials for this purpose, as their amino acid sequences can be engineered to emulate the functional motifs found in proteins. In this thesis project, a laminin-mimetic peptide-based hydrogel was used for the treatment of acute muscle injury.

2.8. Peptide Nanofiber Gels for Muscle Regeneration

Natural ECM contains a complex network of signals that interact with each other to organize cellular behavior and responses. Considering their natural biocompatibility and adaptable characteristics, peptide amphiphiles are ideal as functional tools for designing artificial extracellular matrix-like scaffolds[52]. It is possible to design a complex nano-network system through programmed self-assembly, which is driven by several non-covalent interactions[53]. Under physiological conditions, higher-order complex nanostructures are formed from primary amino acid sequences and replicate the biochemical characteristics and architecture of native tissue. Owing to their special characteristics, peptide amphiphile molecules are excellent bioactive scaffold candidates for tissue engineering and regenerative medicine applications[54, 55].

A peptide sequence derived from the active site of laminin was previously shown to provide an environment similar to that found in the basal lamina of skeletal muscle. The laminin-mimetic PA (LM/E-PA) was also shown to be biocompatible and support the adhesion, growth and differentiation of myoblasts[56]. The LM/E-PA scaffold system has

further been shown to not inhibit the differentiation of the satellite cells, making it an ideal candidate for *in vivo* experiments for the scaffold-mediated repair of muscle injury.

3. Experimental Section

3.1. Materials

9-Fluorenylmethoxycarbonyl (Fmoc) and *tert*-butoxycarbonyl (Boc) protected amino acids, lauric acid, [4-[α-(2'4'-dimethoxyphenyl) Fmoc-amino methyl] phenoxyl] acetomidonorleucyl-MBHA resin (Rink amide MBHA resin), Fmoc-Asp (OtBu)-Wang resin and 2-(1H-benzotriazol-1-yl)-1,1,3,3-tetramethyluronium hexafluorophosphate (HBTU) and diisopropylethylamine (DIEA) were purchased from Merck, NovaBiochem, Sigma-Aldrich and ABCR. Cover glasses and tissue culture plates were purchased from NEST Biotechnology and Corning. Antibodies were obtained from Abcam. Chondrogenesis Differentiation Kit was purchased from Thermo Fisher Scientific. All other materials and chemicals used in the study were analytical grade and purchased from Invitrogen, Fisher, Merck and/or Sigma-Aldrich. All the chemicals were used as provided.

3.1.1. Animal Model

Animal studies were performed in accordance with the Diskapi Yildirim Beyazit Research and Training Hospital (ADACELL facility) for animal care and handling, according to protocols approved by local and governmental Ethics Committees. 50 male, 2 months old healthy Sprague-Dawley rats were used in this study (n=10), weighing 200-250 g. Male rats were chosen to eliminate the potential contradictory effect of hormonal fluctuations on body in this age range. Rats were housed in standard plastic cages in a temperature and light controlled environment (24 ºC; 12h/12h light/dark cycle) and they were allowed to access food and water throughout the experiment.

3.2. Methods

3.2.1 Peptide Amphiphile Synthesis, Purification and Characterization

Peptide amphiphile molecules were synthesized manually by the standard solid phase peptide synthesis chemistry[57]. Laminin-mimetic PA (LM-PA, Lauryl-VVAGKKIKVAV-Am) was constructed on ring amide MBHA resin and E-PA (Lauryl-VVAGE) was constructed on Fmoc-Asp (OtBu)-Wang resin. Couplings of amino acids were performed with 2 equivalents of amino acids activated with 1.95 equivalents of HBTU, and 3 equivalents of N,N-diisopropylethylamine (DIEA) for one unit of starting resin. Each amino acid coupling proceeded 2 h and cleavage of Fmoc protecting group was performed by treating the solid phase with 20% (v/v) piperidine in dimethylformamide (DMF) for 20 min. After coupling all Fmoc protected amino acids, alkyl tail was attached by using lauric acid addition similarly to amino acid coupling except that coupling time was 4 h. In order to block remaining free amine groups by acetylating the unreacted amine groups after each amino acid coupling, 10% (v/v) acetic anhydride solution in DMF was added and treated for 30 min. After each step, resin was washed with DMF, Dichloromethane (DCM) and DMF respectively (three times each). Cleavage of protecting groups and peptide molecules from the resin was carried out by 95% trifluoroacetic acid (TFA) containing cleavage cocktail (95% TFA, 2.5% triisopropylsilane (TIS), 2.5% water) for 3 h. Excess TFA was removed by rotary evaporation. As a following step, ice-cold diethyl ether was used to precipitate the remaining viscous PA solution overnight at -20 ºC. Diethyl ether was expelled after centrifugation at 8000 rpm for 15 min and the resulting precipitate was dissolved in ddH_2O and freeze-dried for two days.

Lyophilized PA molecules were characterized by liquid chromatography-mass spectrometry (LC-MS) and mass spectrum was obtained with Agilent 6530 quadrupole time of flight (Q-TOF) mass spectrometry with electrospray ionization (ESI) source equipped with reverse-phase HPLC system with Zorbax Extend-C18n 21.2 x 150 mm column for basic conditions and Zorbax SB-C8 21.2 x 150 mm column for acidic conditions. To purify the PA molecules and remove the residual TFA, preparative-HPLC system (Agilent 1200 series) was used with a mobile phase of optimized gradient 0.1% TFA/water and 0.1% TFA/acetonitrile for acidic conditions or 0.1% ammonium hydroxide/water and 0.1% ammonium hydroxide/acetonitrile for basic conditions. 0.1% HCl treatment was processed for positively charged peptide amphiphiles. After purification step, PAs were lyophilized and stored as a powder form at -20 ºC for further use.

3.2.2 Self-Assembled Nanofiber Network Formation

PA solutions were prepared by dissolving in sterile ddH_2O and sonicating for 15 min. In order to form nanofibers, oppositely charged peptide amphiphiles were mixed. Positively charged bioactive LM-PA and negatively charged E-PA (at pH 7.4) were mixed to form nanofiber at 2:3 molar ratio, respectively to have final neutral charge. Mixing process was carried out within the syringe right before injection. To see the difference of gelation ability of the peptides, mixing process was also carried out outside the syringe and viscoelastic properties of the gel was analyzed via oscillatory rheology once more.

3.2.3 Structural and Mechanical Characteristics of Peptide Nanofibers

PA nanofiber network was observed by imaging with a scanning electron microscope (SEM). To prepare the sample, oppositely charged PA solutions (1 wt%) were mixed on the silicon wafer surface to produce gel with neutral charge as explained above. After waiting for 10 min of gelation, hydrogel was dehydrated in graded ethanol solutions (20%, 40%, 60%, 80% and 100% v/v) for 10 min at each step. After dehydration, gel was critical point dried by using Autosamdri®-815B from Tousimis. Dried gel was coated with 6 nm Au/Pd and SEM (FEI Quanta 200 FEG) images were taken by using an Everhart-Thornley Detector (ETD) at high vacuum mode.

For transmission electron microscopy (TEM) analysis, sample preparation was done with the same annealing procedure with 1 mM PA concentration. Nanofiber was imaged with TEM (FEI Tecnai G2 F30 TEM). For sample analysis, 1 mM LM-PA and 1 mM E-PA were mixed at 2:3 ratio. Sample was put on a 200-mesh carbon TEM grid for 1 min followed by 2 wt% uranyl acetate staining for 40 s and drying under flow hood.

In order to probe the viscoelastic properties of the PA network, oscillatory rheology measurement was performed with an Anton Paar Physica RM301 rheometer operating with a 25 mm parallel plate configuration at 25 ºC. Samples of LM-PA and E-PA were mixed within the syringe at 2:3 molar ratio and placed on the lower stage of the rheometer. Measurement was done with 0.5 mm gap distance, 100-0.1 rad/s angular frequency and 0.5% shear strain. Storage moduli (G') and loss moduli (G'') values were scanned and recorded at each strain.

Circular Dichroism (CD) (JASCO J815 CD spectrapolarimetry) was used to analyze the secondary structures of PA molecules. To perform the analysis, 0.2 mM aqueous solutions of peptide amphiphiles were diluted from 1 mM stock solution. For each measurement, 300 μL of the sample was put into a 1 mm quartz cuvette. Scanning was done between 190 nm to 300 nm; data interval and data pitch were 0.1 nm and all measurements were performed with three accumulations. Molar ellipticity was calculated with the data obtained from measurements using the equation: $[\theta] = 100 \times \theta / (C \times l)$, where C is the concentration in molar, and l is the cell path length in centimeters.

3.2.4 Acute Muscle Injury Creation via Toxin Injection

Following the anesthesia with ketamine (100 mg/kg) and xylazine (10 mg/kg), the anterolateral aspect of the hindlimbs were shaved and treated with the aseptic solution. A longitudinal incision was made to expose the tibialis anterior (TA) muscle. TA muscle was injured by the injection of 150 μL (10 μM) cardiotoxin (from *Naja Mosambica Mosambica*). After acute muscle injury formation, the skin was closed with a 4-0 suture. Rats were then randomly divided into 5 groups: day 1, 3, 5, 7 and 14.

3.2.5 Treatment with ECM mimetic PA Network

1 day after the operation, right legs of each animal were treated with 150 μL laminin mimetic PA hydrogel application. Gel was made by mixing LM-PA and E-PA into the syringe. Likewise, left legs of the animals were used as a negative control group and 150 μL physiological saline was applied. In order to inject the hydrogel and physiological saline to the correct location, a longitudinal incision was made so as to be identical to the damaged area. After treatment, the skin was closed with a 4-0 suture. All animals were

carefully evaluated during the first 24 h after operation. No animals were observed to be infected throughout the experimental period.

3.2.6 Behavioral Analysis

In order to see the physical outputs of the experiment, behavioral tests were processed. Animal behavior is directly affected from trauma, that is why we need to check some physical parameters. First thing that we measured is motor action potential of the TA muscle via EMG. Second physical analysis was catwalk step test which measures the stride step length of rats. Step length is related with the TA muscle function because of the dorsiflexion movement. Since behavioral analyses are directly affected by acute injury, by doing these two analyses we can observe the functional recovery of the skeletal muscle.

3.2.6.1 Electromyography

Electrophysiological studies were performed to measure the amplitude of the compound motor action potentials (CMAP). Measurements were taken by using Neuro-MEP-Micro two channels EMG (Neurosoft, Russia) device. Recordings were collected from pre-operation (healthy), right after the operation, day 7 and day 14 post-operation. After anesthesia with ketamine (100 mg/kg) and xylazine (10 mg/kg), evaluation place was cleaned with alcohol and allowed to dry before procedure. Schematic representation of the experimental setup can be seen from Figure 7.

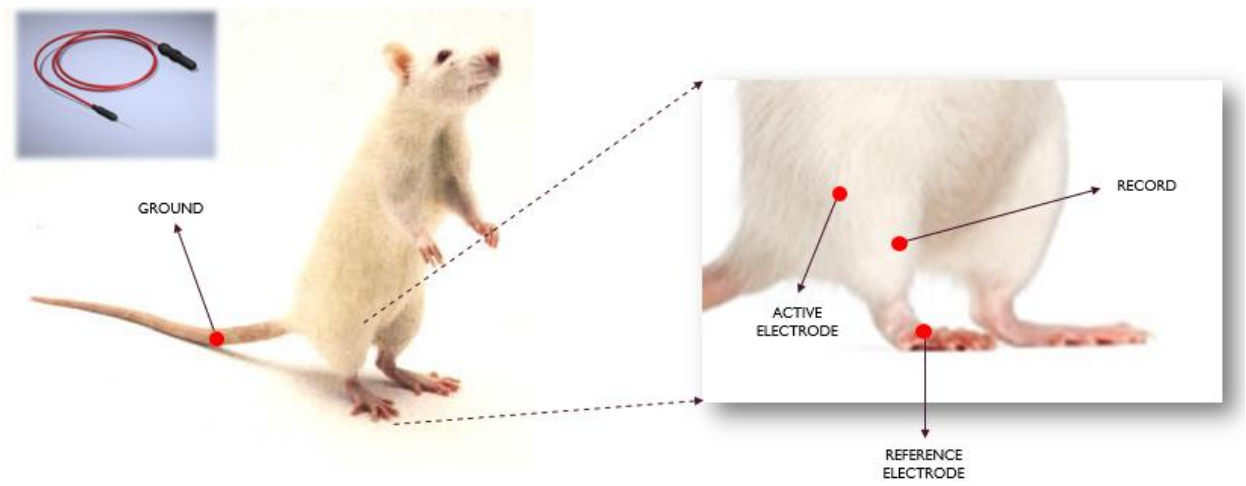

Figure 7 Schematic Illustration of Electromyography Setup. Ground was placed to the tail, reference electrode was placed to the feet, active electrode was placed to the beginning of the leg, and measurements were recorded by using needle electrode from the tibialis anterior muscle.

For this evaluation, recording monopolar needle electrode was placed in TA muscle, reference electrode was placed in dorsum of the foot and common reference (ground electrode) was placed on the tail. In order to observe the amplitude of the motor action potentials sweep speed/sensitivity were set to 4 mV and 4 msec/division. The common peroneal nerve found in the knee at fibula's head was stimulated with bipolar concentric needle electrode. The intensity was gradually increased until dorsiflexion movement was observed and up to supramaximal intensity (current intensity 30% above the value to evoke the maximal CMAP). CMAP amplitude (negative peak's amplitude) was recorded from the TA muscle. Stimulation was repeated 3 times for all measurements and average values were used for statistical analysis.

3.2.6.2 Walking Track Step Test Analysis

At 1, 3, 5, 7 and 14 days after treatment, animals underwent a postoperative behavioral walking-track analysis. The rats were walked over a white sheet of paper (8.2 cm wide, 58 cm long) covering the bottom of a wooden alley ending in a dark destination box. Hind paws of the animals were painted with black ink, and then they were placed into the track to walk. Stride lengths were measured manually as the distance between two pawprints. By considering three longest steps from each walk, stride lengths were calculated[58] and first & last paw prints were excluded because of velocity changes. Obtained data were analyzed and processed in Graphpad software Prism 5, as the mean with SD for each limb. Statistical comparisons were made by paired t-test for paired values and unpaired t-test for unpaired values.

3.2.7 Histological Analysis

3.2.7.1 Morphological Analysis (H&E)

After 1, 3, 5, 7 and 14 days of recovery, 10 rats for each day point were sacrificed and their TA muscles were extracted. TA muscles were divided into 3 pieces in order to proceed with histological, gene expression and protein detection analysis. Tissue allocated for histological examination was put into 4% paraformaldehyde solution for fixation. After 24 h, samples were dehydrated with a graded series of ethanol from 70% to 100% and prepared for paraffin embedding with two changes of xylene. Cleared samples were embedded in paraffin blocks and sectioned at 5 μm thickness by microtome. To assess regeneration, hematoxylin and eosin staining was performed,

slides were mounted by Histomount® mounting medium. Cross-sections were prepared for histological examination on Axio Scope (Zeiss) light microscope.

3.2.7.2 Muscle Cross Section Area Calculation

We next determined the loss of skeletal muscle mass in response to acute injury. Since degeneration causes the depletion of skeletal muscle, cross section thickness of skeletal muscle is associated with the skeletal muscle mass loss. Measurements were conducted at 20X magnification. Per each cross section, five random fields were chosen and area of fibers were calculated by using Image J software. Changes in fiber cross section area between skeletal muscle fibers were determined using parametric (2-way ANOVA) test.

3.2.7.3 Centrally Located Nuclei Calculation

Centrally located myonuclei observation indicates the degree of skeletal muscle regeneration because satellite cells merge with the existing fibers when they are stimulated for regeneration. By the time, they merged with the fibers and located the center of the skeletal fibers. Thus, I calculated the centrally located myonuclei for each group. Measurements were conducted in day 7 at 40X magnification per each cross section by bright-field microscopy. The number of central nuclei per muscle fiber was determined by counting a minimum of five random muscle fiber images per animal and five animals from each group were analyzed. Percentage of myofibers with central nuclei were calculated and statistical analysis was done by using parametric t-test.

3.2.8 Gene Expression Analysis by RT-qPCR

For analyzing molecular level myogenic differentiation, gene expression profiles of skeletal muscle tissue samples were assessed by quantitative real time PCR (qRT-PCR) method. Myogenesis markers such as Pax7, MyoD1, Myf5 and Myogenin were used for this experiment.

3.2.8.1 RNA Isolation

Tissue parts allocated for gene expression analysis were put into test tubes right after animals were sacrificed and immediately frozen with liquid nitrogen. RNA from each sample was isolated with TRIzol reagent (Invitrogen) according to the manufacturer's instruction. Tissues were smashed with a tissue grinder and homogenized with TRIzol reagent by using homogenizer. After homogenization, centrifugation was performed at 4ºC with 2000 G for 5 minutes in order to get rid of tissue debris. 1 mL of supernatant from each sample was taken and 200 µL of chloroform was added into the test tube. Tubes were incubated for 3 min at room temperature and then centrifugation was done for 17 min with 15000 rpm at 4°C. After centrifugation, upper clear phase from each tube was taken and put into a new test tube for ½ v/v isopropanol would be added. 15 times gentle shaking (upside-down) was done and tubes were incubated for 10 min inside the ice container. Next, tubes were centrifuged for 12 min with 15000 rpm at 4 °C and then supernatant was discarded for further steps. Pellets were washed via slowly addition of 70% cold ethanol and tubes were centrifuged at 8000 rpm at 4 °C. Second washing step was applied via slowly addition of 100% cold ethanol and tubes were centrifuged at 8000 rpm at 4 °C again. Tubes were allowed to dry in order to get rid of

ethanol from the samples and 20 µL of DNAse & RNAse free ddH_2O was added to each test tube.

3.2.8.2 RNA Quantification

Purity and yield of isolated RNA were determined with Nanodrop 2000 spectrometer (Thermo Scientific). This system allows us to determine the concentration of RNA by using only 1 µL RNA sample. After quantifying the concentration, purity of RNAs was checked by considering the absorption ratio between 260/280 and 260/230. 260/280 ratio gives an information about protein contamination and should be between 1.8 - 2.0. However, 260/230 ratio gives an information about EDTA, TRIzol and phenol contamination and it should be in between 1.8 - 2.2. In this thesis project, we used only pure RNA for qRT-PCR.

3.2.8.3 Quantitative reverse transcription PCR (RT-qPCR)

Both cDNA synthesis and qRT-PCR were performed with one-step qRT-PCR kit (SuperScript III Platinum SYBR Green) according to the manufacturer's instructions. Primer sets that were used in this project are represented in Table 1 below.

Table 1 Skeletal Muscle Specific Primer Sequences for RT-qPCR

Primer	Sequence (Forward)	Sequence (Reverse)	Annealing Temp.	Efficiency
Pax7	GTGCCCTCAGTGAGTTCGATT	GGGAGGTCGGGTTCTGATTC	59 °C	101.6 %
MyoD1	CATAGACTTGACAGGCCCCG	GCAGGTCTGGTGAGTCGAAA	59.2 °C	102 %
Myf5	AACCAGAGACTCCCCAAGGT	AGCACATGCATTTGATACATCAGG	58.6 °C	97 %
Myogenin	TGGTCCCAACCCAGGAGATC	AGAAGTGGTGGCGTCTGAC	60 °C	97 %
GAPDH	GTGCCAGCCTCGTCTCATA	AACTTGCCGTGGGTAGAGTC	57 °C	96.3 %

Reaction conditions were briefly as follows: 55 ºC for 5 min and 95 ºC for 5 min were applied as a first step. Polymerase chain reaction continued with 40 cycles of 95 ºC for 15 s, 60 ºC for 30 s and 40 ºC for 1 min. Product specificity was confirmed by following a melting curve and the reaction efficiencies for each primer set were evaluated with standard curve using 5-fold serial dilutions of total RNA. For the analysis of expression, primary gene expression data were normalized by the expression level of healthy group and the expression level of GAPDH. A comparative Ct method was used to analyze the results.

3.2.9 Protein Detection by Western Blotting

For detecting myogenic differentiation related proteins, protein profiles were assessed by western blot. Tissue part allocated for protein detection was put into a test tube right after animals were sacrificed and immediately frozen with liquid nitrogen. Total protein from each sample was homogenized with RIPA buffer. Ingredients of the RIPA buffer are presented in Table 2 below.

Table 2 Content of RIPA Lysis Buffer

Chemical	Amount
Tris-HCL (pH: 8.0)	10 mM
EDTA	1 mM
EGTA	0.5 mM
SDS	0.1%

NaCl	140 mM
Triton X-100	1%
Sodium deoxycholate	0.1%
Protease Inhibitor Cocktail	According to the manufacturer's instructions

Proteins were denaturated, resolved on 12% SDS-PAGE and transferred to polyvinylidene difluoride membranes (Thermo Scientific). Membranes were blocked with 5% freeze-dried nonfat milk in TBS-T for 1 h at room temperature and then incubated with primary antibody at 4 ºC overnight. Afterwards, membranes were washed extensively with TBS-T and incubated with HRP conjugated secondary antibody for 1 h and visualized by enhanced chemiluminescence (Bio-Rad) according to the manufacturer's protocol on ChemiDoc™ Imaging System with Image Lab™ Software - Bio-Rad.

3.2.9.1 BCA Assay

Protein concentrations were determined with BCA Assay (Thermo Scientific). BCA is a bicinchoninic acid based colorimetric detection for proteins. Standards for BCA assay was prepared via serial dilution from bovine serum albumin (BSA) and known concentration gradient was obtained in the 2000-0 µg/µL range were prepared. 25 µL of each sample was put into a microplate and 200 µL developing solution (which was prepared from BCA protein assay kit, for 200 µL; 196 µL BCA reagent A + 4 µL BCA reagent B were mixed) was added onto samples. Microplate was incubated at 37 °C for

30 min and absorbance was measured at 560 nm. By using BSA standard curve, unknown concentrations of samples were determined. Protein stock samples were diluted so as to reach 50 µg/mL final concentration for SDS PAGE.

3.2.9.2 SDS PAGE

Molecules are separated according to their molecular weight with SDS Polyacrylamide Gel Electrophoresis technique. Two different acrylamide gel systems were used in these experiments. Stacking gel helps proteins to stack prior to separation. Separating gel is responsible for separation of proteins by their size. Contents of stacking and separating gels are represented in Table 3 below. Protein separation by SDS-PAGE gives an information about the molecular mass of the proteins, and also purity of proteins can be determined by this technique.

Table 3 Contents of Stacking and Separating Acrylamide Gels

Components	4% Stacking Gel	12% Separating Gel
Tris/HCl, 0.5 M (pH 6.8)	1250 µL	-
Tris/HCl, 1.5 M (pH 8.8)	-	2500 µL
ddH_2O	3145 µL	4290 µL
Acrylamide / Bis (37:1)	500 µL	3000 µL
10% SDS	50 µL	100 µL
10% APS	50 µL	100 µL
TEMED	5 µL	10 µL

For preparation of 10 mL of 12% separating gel, 4290 µL of ddH_2O, 3000 µL of Acrylamide / Bis (37:1), 2500 µL of 1.5 M Tris/HCl (pH 8.8), 100 µL of 10% SDS, 100 µL of 10%APS and 10 µL TEMED were mixed. TEMED and APS were added at the end, because they cause faster polymerization of gel.

Separating gel was poured between the PAGE glasses and approximately 2 cm empty space was allowed. Isopropanol was added into such space to remove bubbles and obtain flat gel surface. After 15 min of polymerization, 4% stacking gel was prepared by mixing 3145 µL of ddH_2O, 500 µL of Acrylamide / Bis (37:1), 1250 µL of 0.5 M Tris / HCl (pH 8.8), 50 µL of 10% SDS, 50 µL of 10%APS and 5 µL TEMED.

Isopropanol was removed from separating gel and stacking gel was poured. Next, comb was placed into stacking gel and allowed for polymerization for 15 min. 35 µL of protein samples were prepared to obtain 50 µg/mL final protein concentration. For this purpose, 6X Laemmli loading dye and ddH_2O were used. Protein solutions were incubated at 95 ºC for 5 min and gels were loaded by putting 4 µL of protein ladder and 30 µL of protein solutions. Separation was processed at 70 V for 20 min and 110 V for 2 h at room temperature. The content of stock running buffer is shown in Table 4 below. While running, ladder was always checked to observe whether its bands separate uniformly or not. In this thesis work, broad ranged (11-190 kDa) Blue Prestained Protein Standard was used (Invitrogen).

Table 4 Content of 5X Running Buffer for SDS-PAGE (1L)

Reagent	Required Amount (for 1 L)
Glycine	95 grams
10% SDS	30 mL
Trizma Base	15.2 g
ddH_2O	970 mL

3.2.9.3 Protein Transfer onto a PVDF Membrane

Separated proteins were transferred onto polyvinylidene difluoride (PVDF) membrane after electrophoresis. First, glass plate was opened and stacking gel was removed from the separating gel. In order to transfer proteins from gel to PVDF membrane Semi-Dry Electrophoretic Transfer Cell electroblot system was used. Filter papers were equilibrated in anode and cathode buffers and experimental setup was created as represented in Figure 8. Anode and cathode buffers were prepared from Towbin stock buffer. The content of the buffers are represented in Table 5, 6 and 7 below. To avoid air bubbles, glass tube was rolled onto papers and electroblot was performed at 12 V for 50 min for each gel.

Table 5 Content of 10X Towbin Buffer (Anode and Cathode Buffers are prepared from this buffer)

Reagent	Stock Concentration	Required Amount (for 500 mL)
Tris HCl	2 M	62.5 mL
Glycine	-	72.0672 g
ddH_2O	-	437.5 mL

Table 6 Content of Anode Buffer

Reagent	Stock Concentration	Required Volume (for 100 mL)
Towbin Buffer	10 X	20 mL
Methanol	100%	10 mL
ddH_2O	-	70 mL

Table 7 Content of Cathode Buffer

Reagent	Stock Concentration	Required Volume (for 100 mL)
Towbin Buffer	10 X	10 mL
SDS	10%	1 mL
ddH_2O	-	89 mL

Figure 8 Gel and membrane for semi-dry electrophoretic transfer system.

3.2.9.4 Coomassie Staining

Coomassie blue staining was performed in order to visualize the protein bands and confirm that proteins were transferred properly onto the membrane. The dye can bind to amino acids in acidic conditions; therefore, Coomassie stain was prepared in acidic solution. The content of Coomassie Brilliant Blue is represented in Table 8 below. Polyacrylamide gel was incubated with Coomassie staining solution for 2 h on shaker. Next, gel was put into destaining solution for 1 h as well to remove excess Coomassie dye. The content of Coomassie Destainin Solution is also represented below in Table 9.

Table 8 Coomassie Brilliant Blue Staining Solution Content

Chemicals	Amount
Methanol	500 mL
Glacial Acetic Acid	100 mL
Coomassie Blue	10 mL
ddH_2O	Up to 1 L

Table 9 Coomassie Destaining Solution Content

Chemicals	Amount
Methanol	400 mL
Glacial Acetic Acid	100 mL
ddH_2O	Up to 1 L

3.2.9.5 Antibody Incubation

After protein transfer from gel to membrane, the membrane was blocked using the 5% non-fat milk in TBS-T (blocking solution) in order to prevent non-specific interaction. Content of TBS and TBS-T buffers are indicated in Table 10 and 11 below. Membranes were put into blocking solution for 2 h on the shaker, then, they were incubated overnight after the blocking step.

Table 10 Content of 1X TBS Buffer for Electrophoresis

Reagent	Stock Concentration	Required Amount (for 1 L)
20 mM Trizma Base	-	2.42 gr
137 mM NaCl	-	8 gr
ddH_2O	-	1 L

Table 11 Content of 1X TBS-T Buffer for Western Blotting Applications

Reagent	Stock Concentration	Required Amount (for 1 L)
TBS pH 7.4	1 X	999 mL
Tween-20	-	1 mL

After blocking step, membranes were incubated with primary antibody. Primary antibody specifications and dilutions are indicated in Table 12 below. Primary antibody incubation was done through sealing membranes which allows easy application and reduce the antibody amount that is used for hybridization.

Table 12 Working Concentrations and Catalog Numbers of Primary Antibodies

Antibody	Catalog Number	Dilution	Approximate Band Size
Anti Pax7	LS Biosciences LS-B3490	1:5000	57 kDa
Anti MyoD1	Abcam ab16148	1 µg/mL	35 kDa
Anti Myf5	Abcam ab125078	1:10000	37 kDa
Anti Myogenin	Abcam ab1835	1:250	40 kDa
GAPDH	Millipore MAB374	1:500	36 kDa

Membranes were sealed by using sealing machine and antibody incubation was done at 4 °C. After overnight incubation, membranes were washed with TBS-T and incubated with HRP conjugated secondary antibody for 2 h at room temperature with gentle shaking. Secondary antibody specifications and dilutions are indicated in Table 13 below.

Table 13 Working Concentrations and Catalog Numbers of Secondary Antibodies

Antibody	Catalog Number	Dilution
Anti-rb IgG-HRP	Abcam ab6721	1:2000
Anti-m IgG-HRP	Millipore 12-349	1:1000

3.2.9.6 Visualizing Results

After applying the secondary antibodies, membranes were washed twice with TBS-T, before applying the 20X BIO-RAD enhanced chemiluminescence (ECL) reagent for detection of the proteins. ECL solution was incubated for 5 min in dark environment at room temperature, and then membranes were placed in BIO-RAD Chemi-Doc imaging system detector and protocol was followed. The system is controlled by Image Lab™ software to optimize imager. In order to quantify images, ImageJ software was used. GAPDH bands were also analyzed to normalize the results.

3.2.9.7 Blot Stripping

In order to strip away the attached antibodies from the membrane, Blot Stripping Buffer (pH 2.2) was used, and this buffer was prepared by using chemicals that are listed in Table 14 below.

Table 14 Content of Blot Stripping Buffer

Reagent	Required Amount (for 1 L)
Glycine for electrophoresis	15 g
SDS	1 g
Tween 20	10 mL
ddH_2O	Up to 1 L

For reutilizing the membranes, stripping was an essential part of the experiments. For this purpose, first the membranes were kept in stripping buffer for 10 min, twice with a washing out in between. Then, they were kept in PBS Buffer for 2 x 10 min. Ultimately, the membranes were moved into TBS-T buffer and were incubated for 2 x 5 min, before the reapplication of the blocking step followed by the application of the primary antibodies.

3.2.9.8 Quantification and Statistical Analysis

Results were expressed as mean ± standard deviation. Either one-way analysis of variance (ANOVA) or two-way ANOVA with *Tukey's* / *Bonferroni's Multiple Comparison Test* (GraphPad Prism v5) was used to compare values between the study groups. Paired and nonpaired *t*-test were also applied to describe the association between the study groups. A value of $p \leq 0.05$ was considered statistically significant. Error bars indicate the standard error of the mean.

4 Results and Discussion

4.2 Synthesis of PA Molecules and Characterization of Their Self-assembly into Nanofibers

In order to study skeletal muscle regeneration supporting ability, laminin mimetic PA (LM-PA) and E-PA were designed (Figure 9) and synthesized. E-PA was the bioactive epitope free form and, had a hydrophobic alkyl tail consisting of lauric acid and a β-sheet forming peptide sequence, VVAG. Since two oppositely charged peptide molecules can form hydrogels via electrostatic interactions at physiological pH [59], E-PA was used for hydrogel formation with oppositely charged PAs to obtain LM/E-PA nanofibers. On the other side LM-PA molecule is decorated with laminin derived sequence "IKVAV" to generate a myogenic nanofibrous environment suitable for the myogenic differentiation of the satellite cells from skeletal muscle in *in vivo* animal model. LM-PA was previously shown to induce myogenic differentiation of C2C12 myoblast model cells[56]. All PAs were synthesized by solid phase peptide synthesis method. At pH 7.4, LM-PA has a net charge of +3, whereas E-PA bears a -2 net charge. During self-assembly, hydrophobic collapse is induced by the help of alkyl tails and β-sheet forming VVAG sequence induces nanofiber formation[60]. By mixing with 1% negatively charged and positively charged peptides at pH 7.4, self-assembly was triggered. Mixing was processed with a volume ratio of 2:3 (LM:E) in order to end up with a neutral net charge.

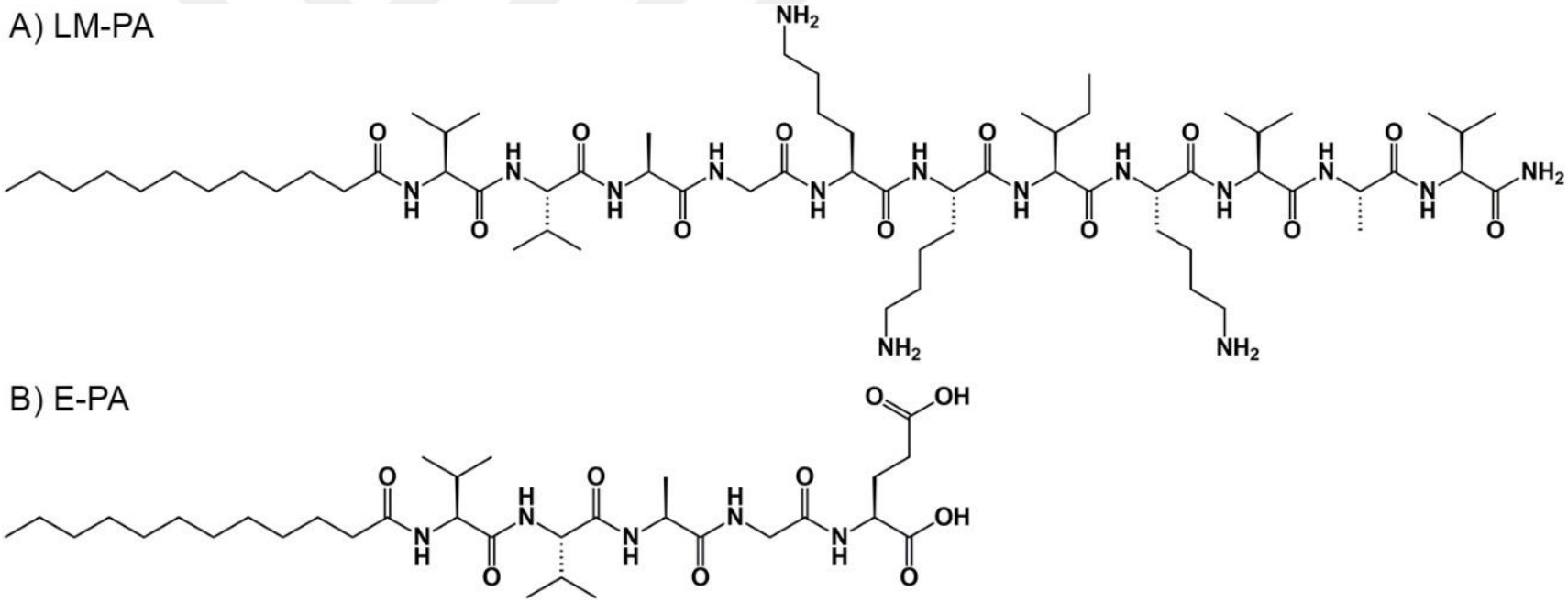

Figure 9 Chemical structures of peptide amphiphile molecules (PAs). A) LM-PA, Lauryl-VVAGKKIKVAV-Am, B) E-PA, Lauryl-VVAGE-OH

4.3 Structural and Mechanical Characteristics of Peptide Nanofibers

After mixing peptides, the abilities of peptides to form a nanofiber network, which also can mimic the architectural properties of the natural ECM were analyzed. To visualize the complex nanofibrous and porous network formation of peptide amphiphile mixtures, scanning electron microscopy (SEM) and transmission electron microscopy (TEM) were used (Figure 10).

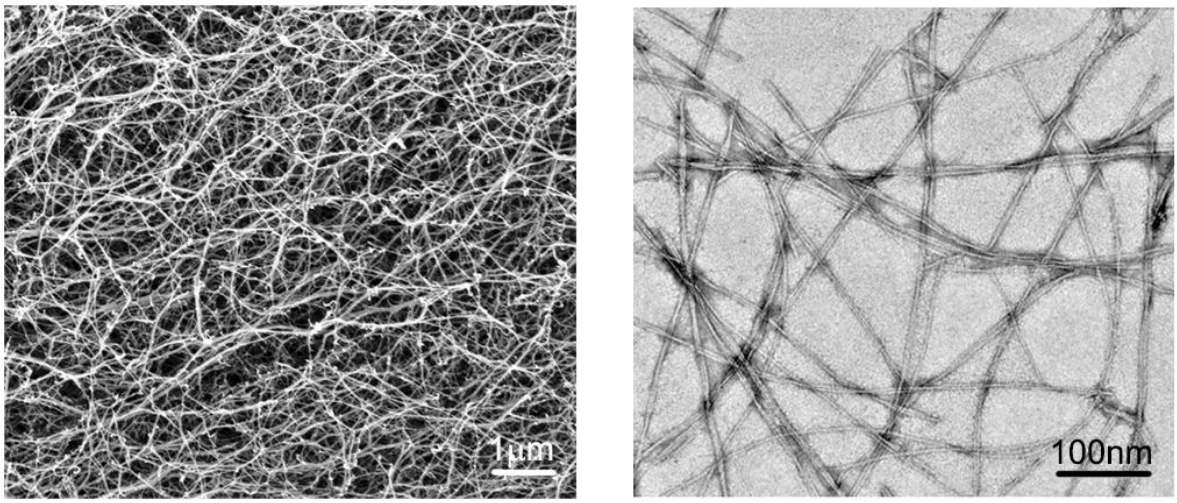

Figure 10 Structural characterizations of PAs by using Scanning Electron Microscopy and Transmission Electron Microscopy. (Left) Representative SEM image of LM/E-PA, (Right) Representative TEM image of LM/E-PA.

After self-assembly, both organized structure and individual nanofibers were observed by SEM and TEM. Peptides were purified with HPLC and characterized by LC/MS (Figure 11).

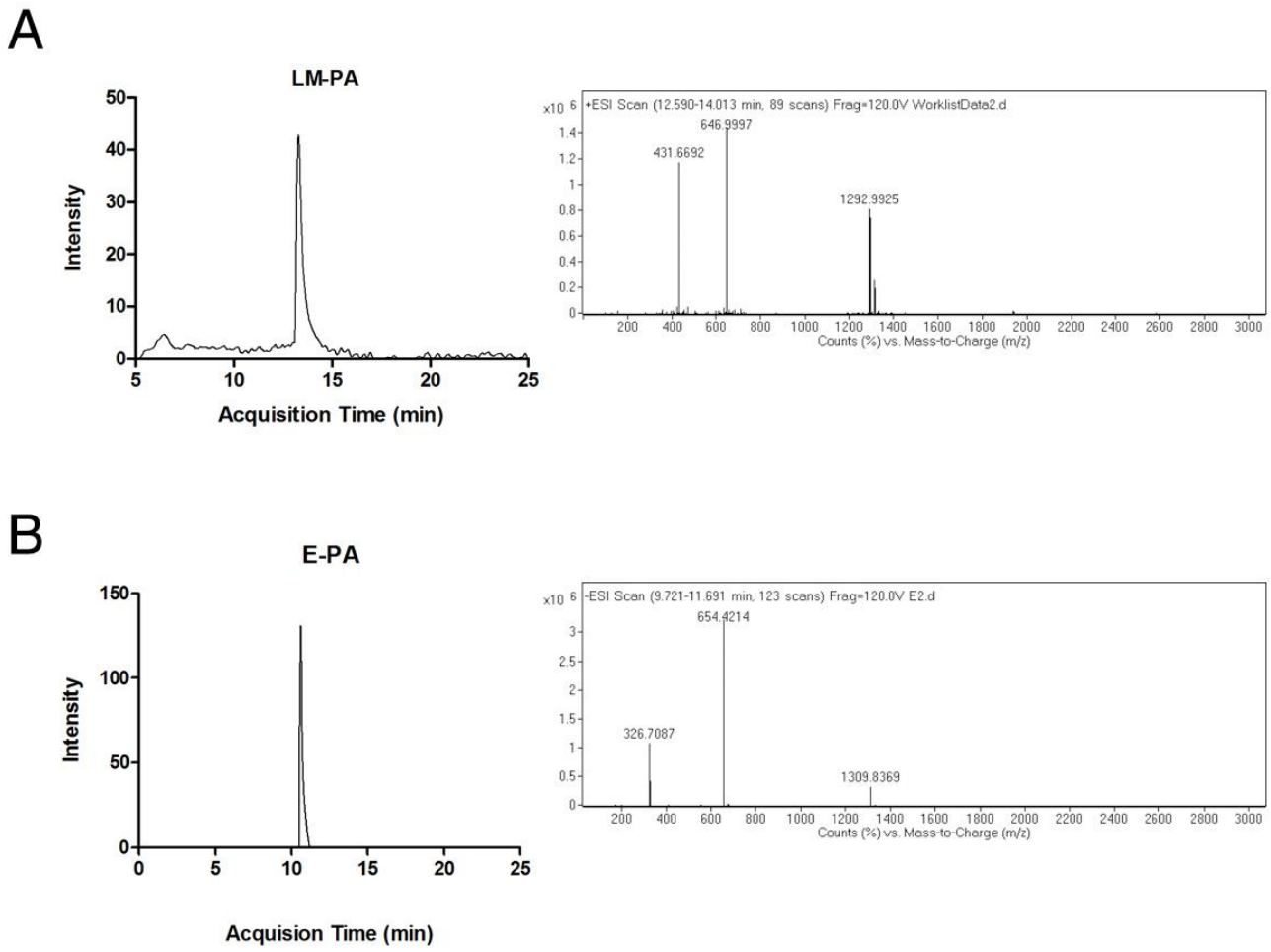

Figure 11 Liquid chromatograms and mass spectra of PAs. (A) LM-PA, $[M+H]^+$ (calculated) =1291.93, $[M+H]^+$ (observed) = 1292.99 (observed $[M/2+H]^+$ = 646.99 and observed $[M/3+H]^+$ = 431.66). (B) E-PA, $[M-H]^-$ (calculated) = 654.4156, $[M-H]^-$ (observed) = 654.42 (observed $[M/2-H]^-$ m/z = 326.70, $[2M-H]^-$ m/z = 1309. 83).

We also performed circular dichroism (CD) analysis (Figure 12) to characterize the secondary structures of peptide amphiphiles and their mixtures. LM-PA and LM/E-PA show β-sheet structure with a minimum around 220 nm and maximum around 200 nm.

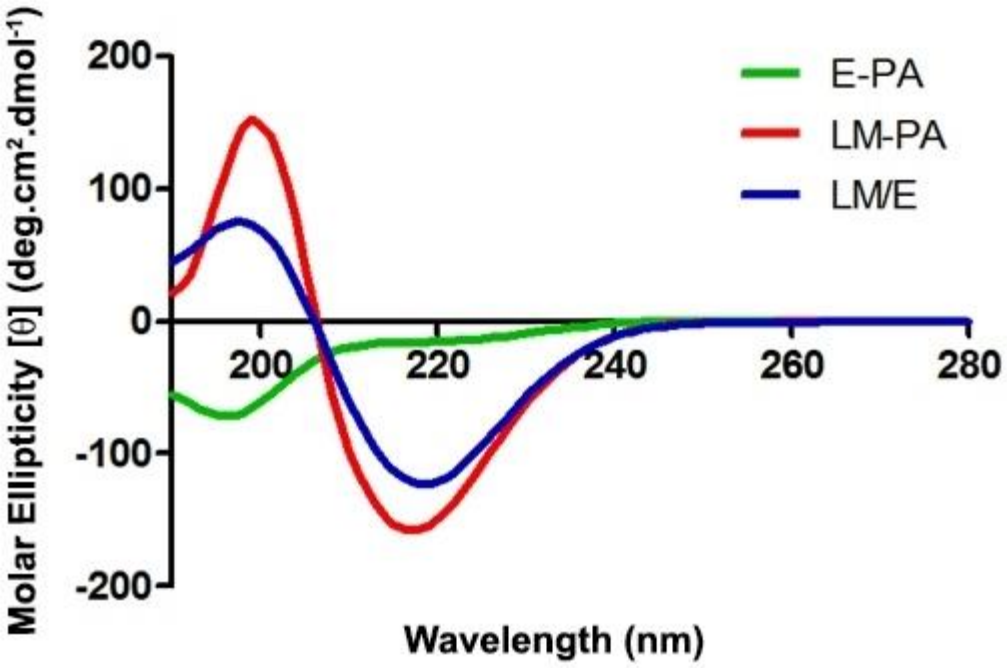

Figure 12 Secondary structure characterization of PAs by using circular dichroism. LM/E-PA combination shows beta-sheet secondary structure.

Oscillatory rheology was employed in order to characterize the mechanical properties of the gel (Figure 13A). Gel formation was confirmed via this method. We also checked whether mechanical properties change with the mixing method, so we took another measurement by mixing peptides outside the syringe (Figure 13B). We again monitored gel structure, but this time stronger form of gel was achieved.

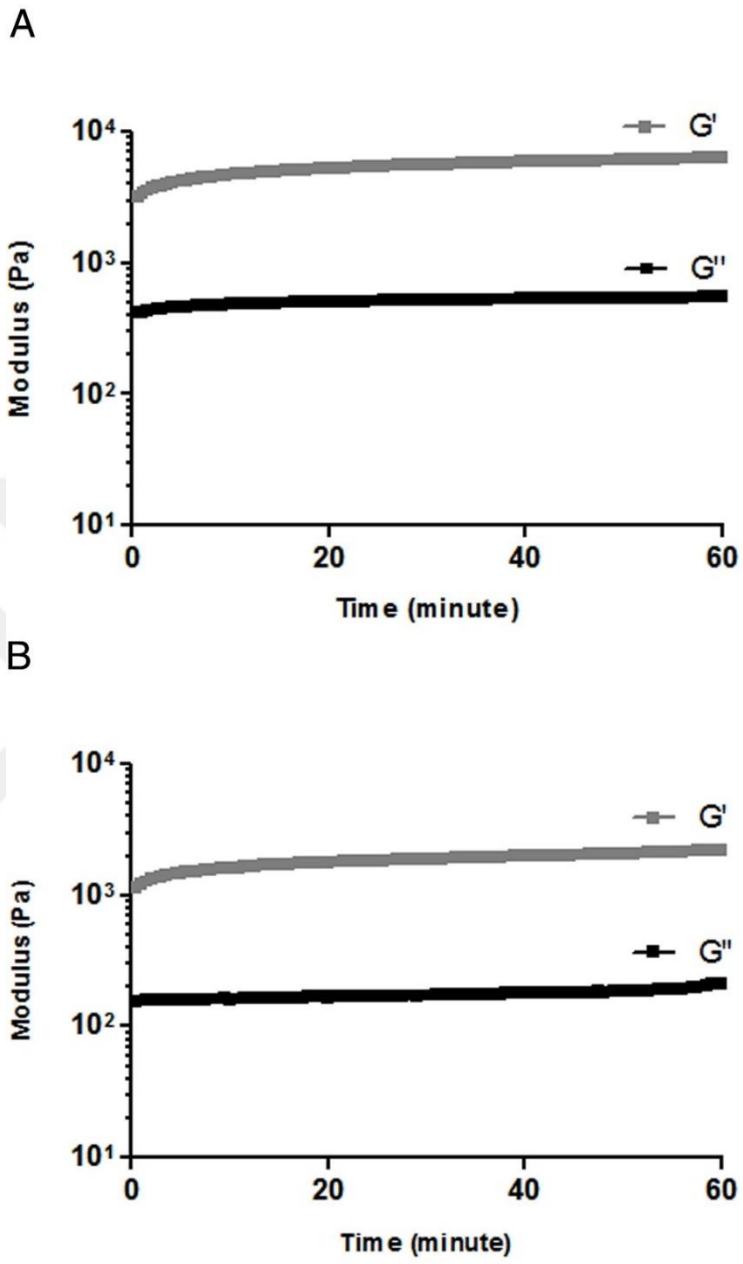

Figure 13 Mechanical characterization of PAs by using oscillatory rheology. A) Storage and loss moduli of LM/E-PA. Peptides were mixed outside the syringe before taking measurements. B) Storage and loss moduli of LM/E-PA. Peptides were mixed inside the syringe before taking measurements.

4.4 Animal Behavior Analyses

4.4.1 Step Test Results

Acute muscle injuries were created in both right and left legs and treated with either LM/E-PA gel (right leg) or the injection of physiological saline as a negative control (left leg). The recovery process was evaluated by step test on days 1, 3, 5, 7 and 14. Schematic of a step test is represented in Figure 14.

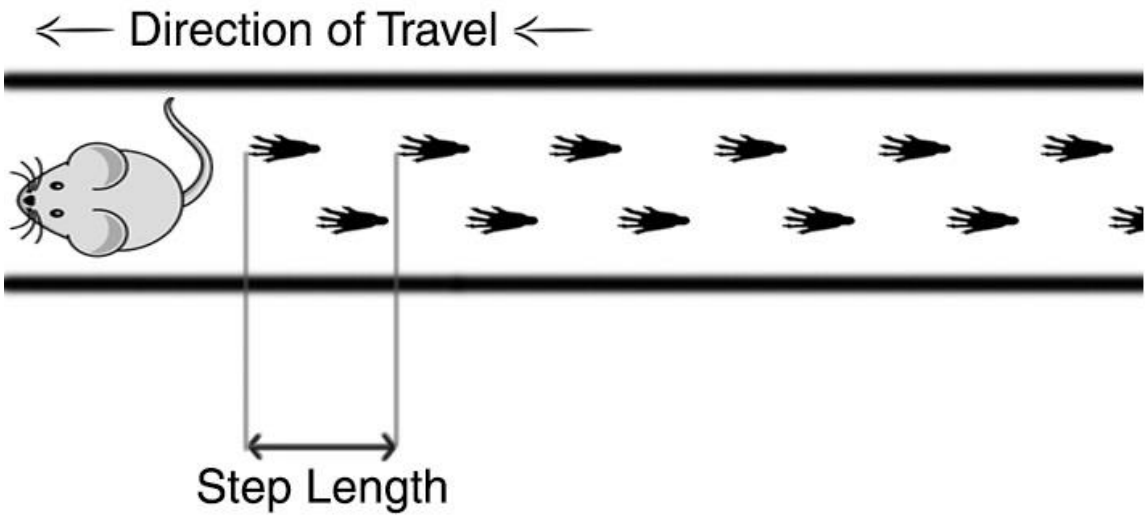

Figure 14 Schematic illustration of step test cabin and experimental

In this experiment, hind paws of the rat were painted with black ink and the animal was walked through the straight cabin. The rat was required to reach the dark box at the end of the straight walk. If the rat walked consistently and provided more than three consecutive step cycles, the measurements were considered to be fit for analysis. Step lengths were measured using the imprints left by the animal following its walk. The results are presented in Figure 15.

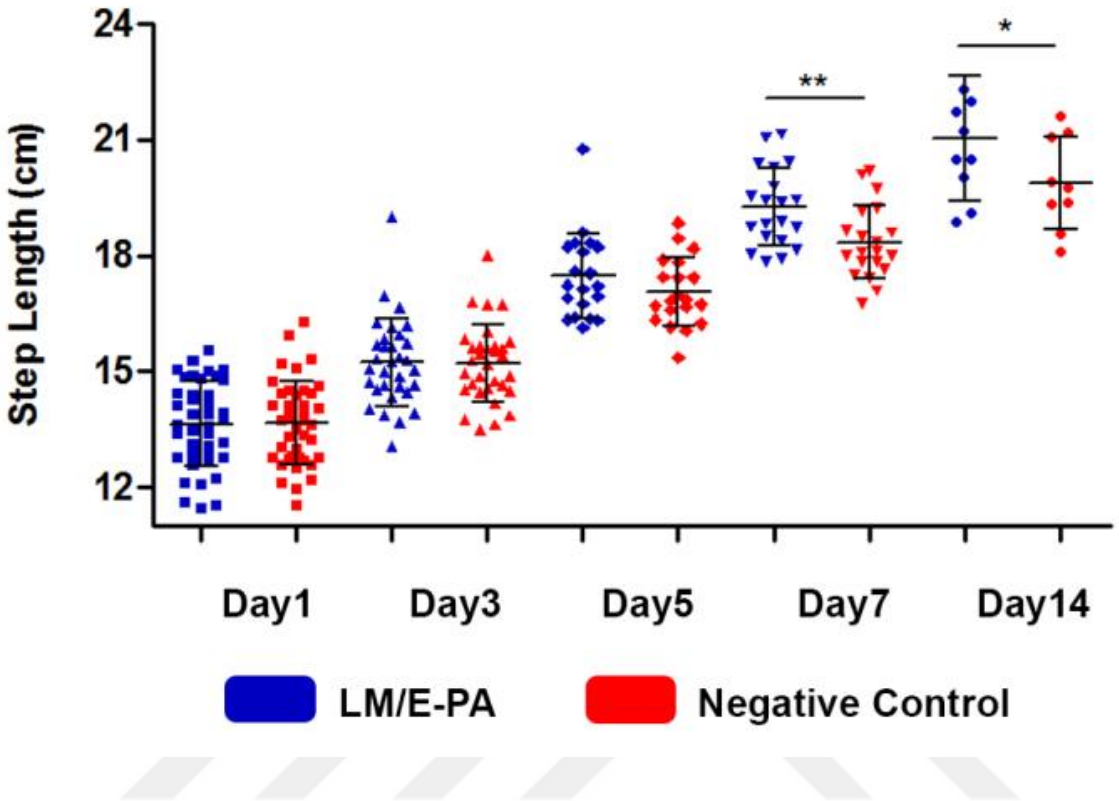

Figure 15 Quantitative step length analyses of both PA and negative control (physiological saline treated) groups. Error bars represent mean ± SD (**p<0.01, *p<0.05)

According to these results; on day 7, the PA-treated group shows nearly the same amount of functional recovery with the day 14 saline-treated group. Lower step lengths are typically associated with higher cell loss and functional reduction[58]; consequently, step length measurements are a promising tool for detection of the functional deficiencies in rodents. During first 5 days of the experiment, no significant differences were observed between the step lengths of both legs, possibly because of the acute muscle trauma. Identical injections were performed on both limbs of the test animals; as such, no difference is expected between the trauma-mediated losses in mass and function

between the PA- and saline-treated muscles. However, on day 7 and day 14, significant differences were observed between the PA- and saline-treated groups. This is an expected result, because functional recovery differences usually show their effects at later stages. We also controlled the animal velocity by observation and found that all animals walked with the same velocity. The animals were also not observed to run during the course of the experiments; all animals were observed to maintain an identical walking gait. Animals that walked less than 3 steps were not considered for this experiment and made to walk again. Despite the reduction of the number of animals at later stages of the experiment, significant differences were present only at the 7^{th} and 14^{th} days, suggesting that our observations are due to genuine differences in muscle recovery patterns. Since the TA muscle is responsible for the dorsiflexion movement[61], stepping behaviors of animals were directly affected by the injury. In this respect, it can be indicated that this animal and injury model is also reproducible. As a conclusion, it can be said that LM/E-PA gel provides increased amount of functional recovery in long term.

4.4.2 EMG Results

Muscle recovery was also quantified by electromyographical (EMG) analysis at four time points; pre-operation (healthy), right after the operation (day zero), day 7 and day 14 post-operation. As the distance between measuring electrodes is known to considerably alter the measurements[62], animals were marked with tissue dye at specific "measurement sites" and electrodes were only inserted at these regions. As the TA is a voluntary muscle, animals were anaesthetized prior to measurements to ensure that no

voluntary movements had taken place. Our EMG results can be seen from Figure 16, as indicated below.

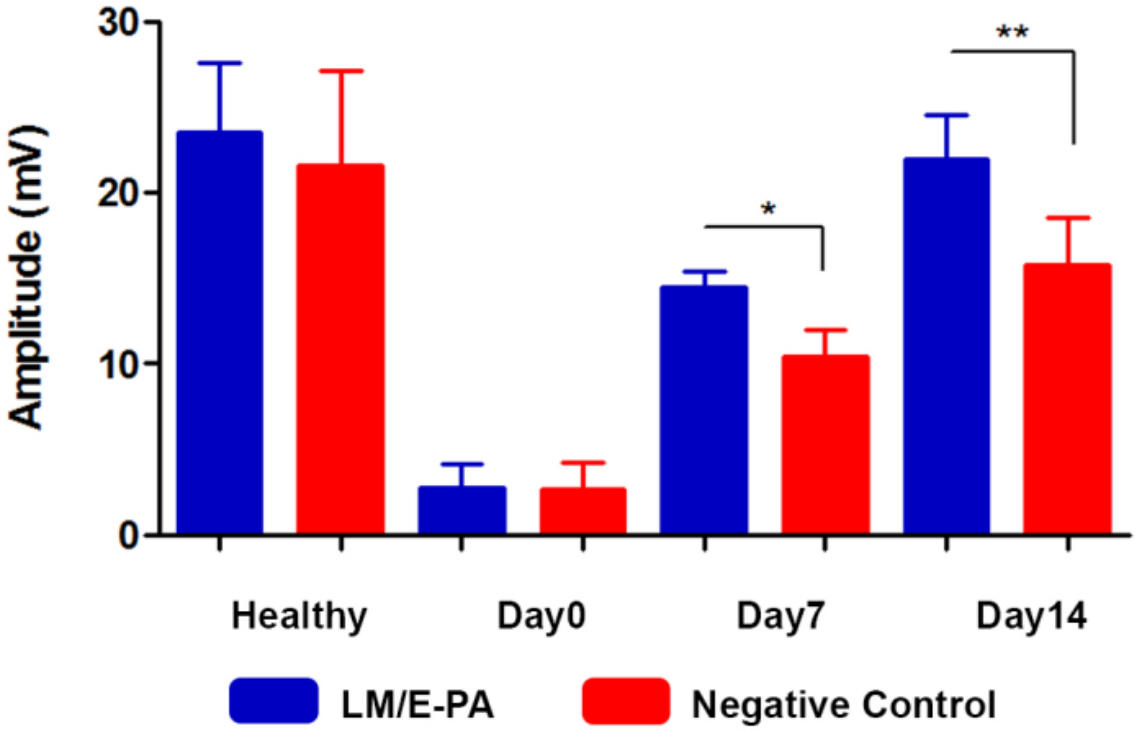

Figure 16 Electromyography (EMG) results show that PA-treatment increases muscle action potential at 7th and 14th days. Error bars represent mean ± SD, n=10 (**p<0.01, *p<0.05)

No significant differences were observed between the EMG results of right and left legs for healthy animals, suggesting that the measurement method is accurate. Moreover, highest amplitude values were observed in the healthy group which is also consistent with our expectations. After cardiotoxin (CTX) injection, the amplitude for both right and left legs drastically decreased and no significant difference was observed between

the two legs, confirming that an acute muscle injury was successfully created on both legs. The minimum amplitude values were measured in this post-operation group and this information confirms that skeletal muscles were barely functional after acute muscle injury. It can be also said that this injury causes equal functional loss in both right and left legs, as no significant differences were observed between the amplitude values of both limbs. When we look at the 7th day EMG data, it can be clearly seen that PA-treated group gives significantly higher amplitude values than the saline treated group. This value also seems to be almost the same with the saline-treated group on the 14th day results. As such, the peptide scaffold appears to restore muscle function more rapidly than physiological saline, such that 7 days of PA treatment is equivalent to 14 days of saline treatment. On the other hand, the 14th day PA data showed us almost equal amplitude results with the healthy group, which is a striking result, as complete healing typically occurs 3-4 weeks after injury[63]. It should nevertheless be noted that PA results are still slightly inferior to healthy muscle, as 14 days of recovery is not sufficient for the complete regeneration of skeletal muscle. Electromyography is a good procedure to measure the motor action potential[64] and our EMG data also agrees with the catwalk step test results. Functional recovery and statistical significance can be consistently observed after the first week. In conclusion, our EMG results demonstrate that the PA-treated group mediates the formation of higher-amplitude compound motor action potentials after the first week of treatment. Therefore, physiological functions are recovered in the PA group to a much greater extent than the saline group.

4.5 Histological Analyses

We also investigated the histological appearance of muscle fibers on days 1, 3, 5, 7 and 14 after PA treatment (Figure 17). Degeneration started on day 1 and reached its highest level on day 3, such that the muscle cross section area could not be measured on day 3. Regenerating fibers became apparent on day 5 and the successive steps of muscle regeneration could be observed in tissue sections for 14 days.

Histological analysis of regenerating fibers indicated greater increase in fiber diameters following LM/E-PA treatment compared to the saline-treated control group. After 14 days of regeneration, nearly all of the injured area was regenerated through the merging of the satellite cells with the muscle fibers. This suggests that the regenerated fibers were present in both groups; however, muscle regeneration was more extensive in the PA group compared to the control group at the end of the experimental period.

We studied the developments in muscle fiber regeneration at different time points (days 1, 3, 5, 7 and 14) following acute muscle injury creation and LM/E-PA hydrogel injection. H&E staining was used to visualize the individual skeletal muscle fibers, which could not be observed during the initial days of recovery due to the massive fiber loss caused by degeneration[65]. On day 5, muscle fibers started to regenerate and fuse with each other and correspondingly had very small diameters. On day 7, fibers started to organize, bundles got close to each other and, interestingly, the differences between PA and control groups started to become prominent. Finally, on day 14, we saw that muscle fibers were far from each other in the control group when compared to the PA group.

Even at this time point, the PA group presented a more organized and more healthy-like physical structure, suggesting enhanced regeneration *in vivo*. We also performed further analysis from histological images; in particular, cross section area calculations were used to quantify the extent of muscle regeneration.

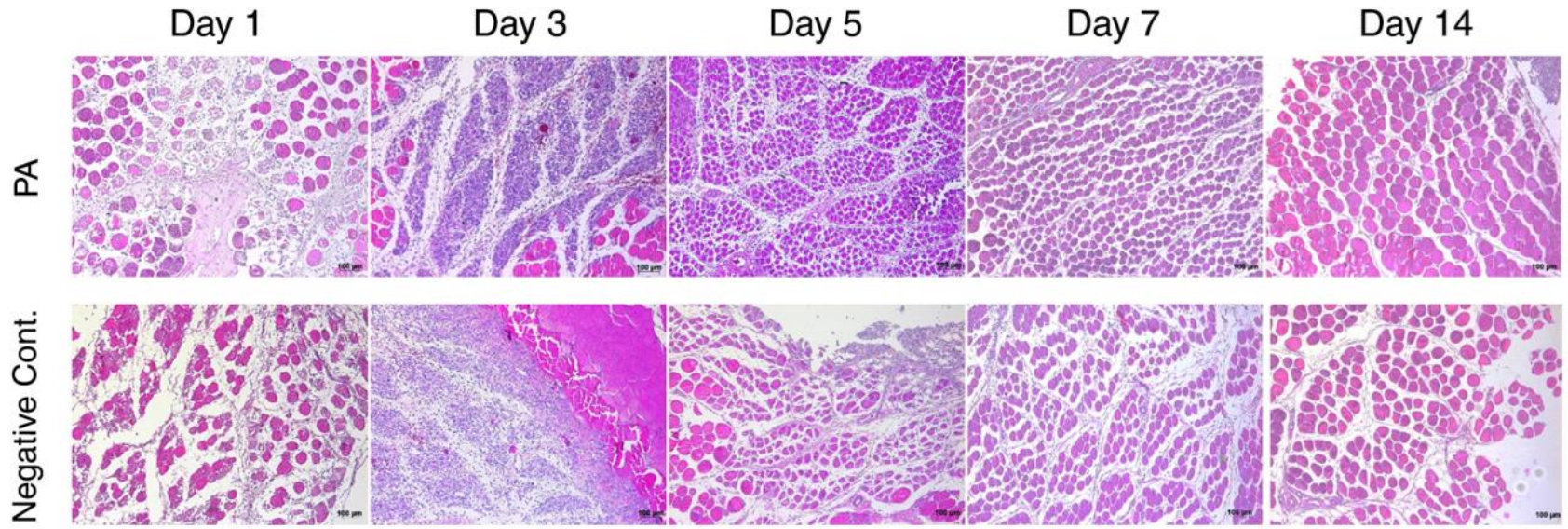

Figure 17 Representative light microscopy images of skeletal muscle tissue sections after H&E staining. Sections were taken on days 1, 3, 5, 7 and 14 in order to follow skeletal muscle regeneration step by step. (Scale bars: 100 μm)

After H&E staining, average muscle cross section areas were also calculated from the images. Our results show that, the LM/E-PA-treated group had thicker fiber cross sections, which means fibers gained better physical recovery after LM/E-PA gel treatment (Figure 18).

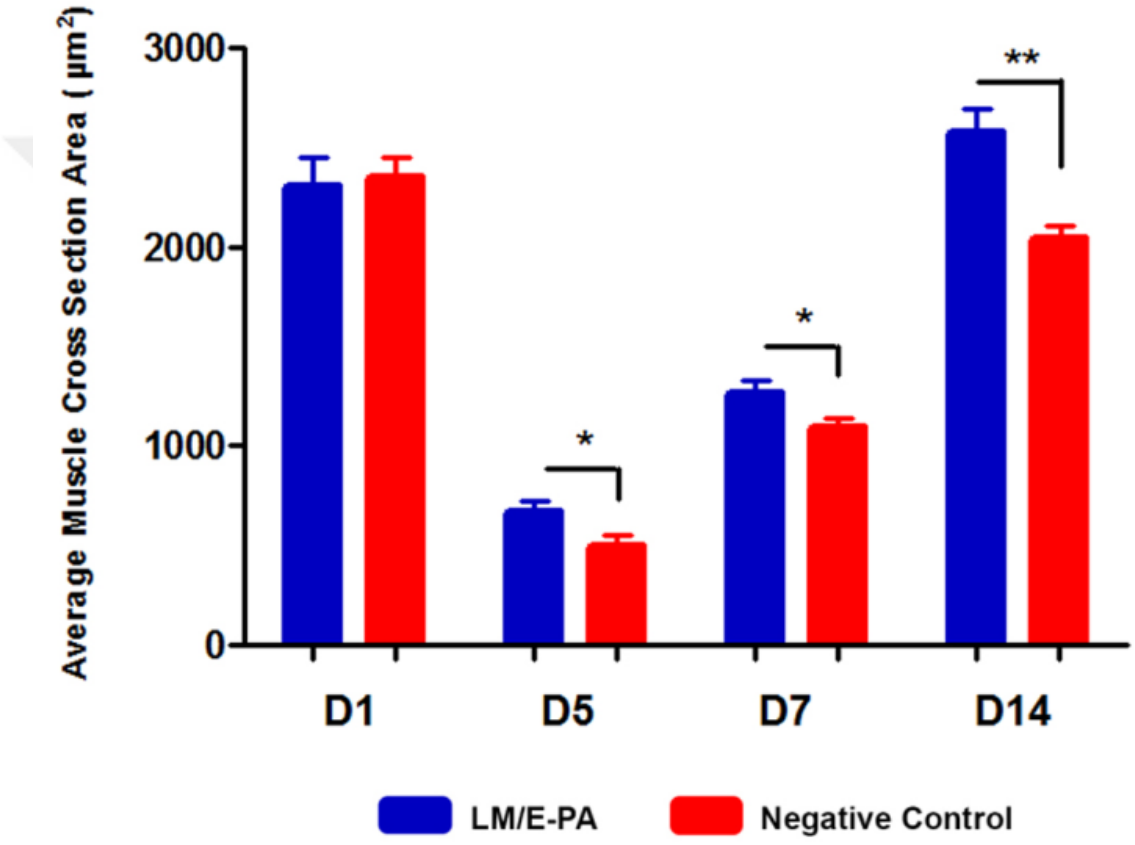

Figure 18 Quantitative analysis of average skeletal muscle cross section area calculation. Error bars represent mean ± SEM, n=5 (**p<0.01, *p<0.05)

Calculation of fiber cross section area per total wound area indicated that the formation of regenerated tissue was faster in the bioactive group on days 5, 7 and 14. Moreover, regenerated fiber formation rates were similar in later days of regeneration (Figure 18). The average muscle cross section area was high in both PA and control groups on day 1, suggesting that injury was not fully created at this point. Although cardiotoxin is a powerful venom toxin, skeletal muscle fiber breakdown is a long-term process; consequently, the disassembly of skeletal fibers was only observed on day 3. Indeed, fiber disassembly was so complete that no cross section area results could be calculated at this time period. Fiber regeneration began on day 5, at which point the average muscle cross section area was higher in the PA-treated group than the saline control. This trend was present for the remaining 9 days, and cross sections of PA-treated muscle fibers were comparable to healthy tissue on day 14. Skeletal muscle cross section area is known to be directly related with the strength and effective capacity of the muscle; as such, higher cross-section areas correspond to healthy skeletal muscle tissue[66]. In conclusion, we can say that PA treatment provides accelerated muscle regeneration because fibers gain their mass in the PA group at a greater rate compared with the physiological saline control group.

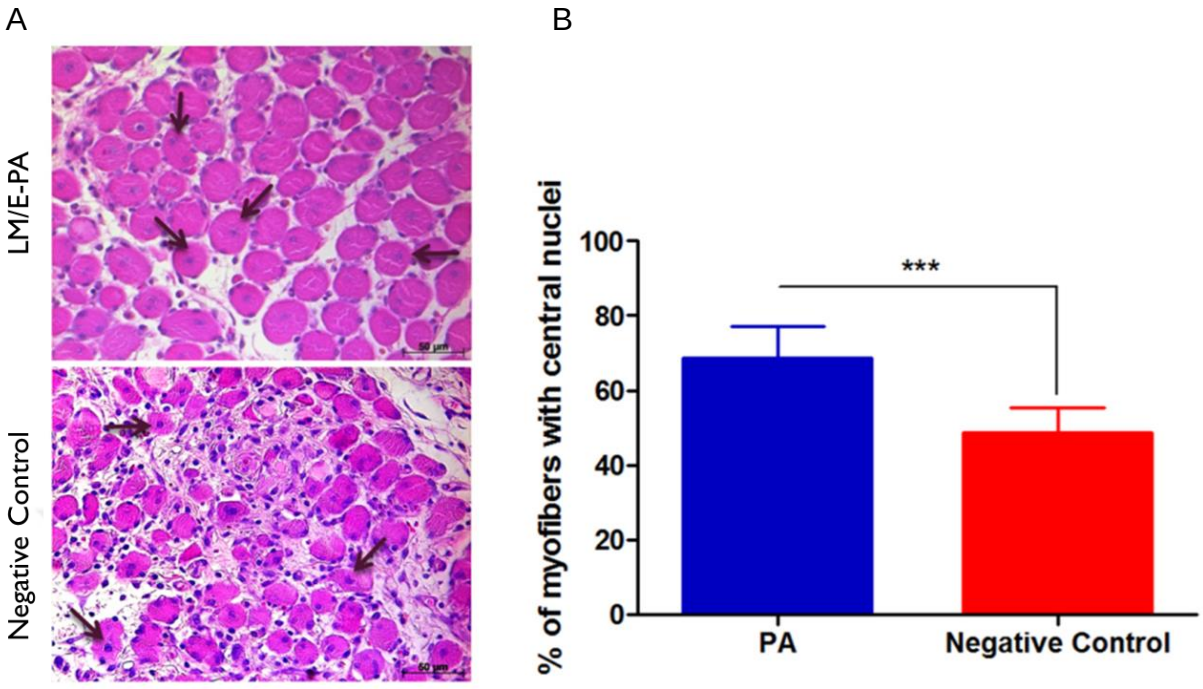

Figure 19 A) Histology images of centrally located nuclei, which correspond to regenerating muscle fibers. B) Quantitative analysis of percentage of myofibers with central nuclei. Bioactive PA injected tissues show increased number of nuclei that were fused with the individual fibers. Error bars represent mean ± SEM, n=5 (***p<0.001, **p<0.01, *p<0.05)

Myofiber repair, which is one of the main markers of skeletal muscle regeneration, was also determined by counting centrally located myonuclei per muscle fiber. Centrally located nuclei images and their quantifications indicate that a greater number of cells merged with the muscle fibers within the same period of time for the PA-treated group (Figure 19). In contrast, several cells were observed to not have merged with each other in the saline-treated negative controls. On the other hand, those satellite cells were almost uniformly merged with the muscle fibers in the PA group and were located at the center of the skeletal muscle fibers. It is known that centrally located myonuclei is a

major indicator of newly regenerated fibers. Continuing myofiber repair causes central nuclei localization and this appearance of myonuclei is only seen in regenerating skeletal muscle fibers[67]. In the present study, we demonstrated that the percentage of myofibers with centrally located nuclei was significantly higher in the laminin-mimetic PA hydrogel-treated group on day 7 compared to saline treated negative control group. This result is consistent with the other histological data and suggests that bioactive hydrogel treatment accelerates skeletal muscle regeneration by facilitating satellite cell activation and fusion of SCs with the fibers. Day 7 data was used for this analysis because individual fibers were easily observed on day 7. We also found that there was no difference between the regeneration capacities on the first days of the experiment. However, when the satellite cells began to be recruited, a clear difference could be observed between the regeneration rates associated with PA-treated and control groups. By considering all these histological analyses, it can be concluded that laminin mimetic PA treatment facilitates the early activation of satellite cells and promotes faster skeletal muscle regeneration.

4.6 Gene Expression Analyses

Skeletal muscle differentiation markers were checked by RT-qPCR in order to observe the genetic underpinnings of the myogenesis process. Four different myogenesis markers that take part in different steps of myogenesis were used in this project: Pax7, MyoD1, Myf5 and Myogenin. By checking these markers, we could further confirm the effects of peptide hydrogels on the regeneration of skeletal muscle, because gene expression profiles of myogenic transcription factors are strongly related with skeletal muscle regeneration.

Pax7 is the main transcription factor that is expressed in satellite cells; as such, it is one of the crucial markers of satellite cells. It is known that Pax7 expression continues even after satellite cells are activated and differentiation begins[68]. This makes Pax7 a good marker for the early steps of skeletal myogenesis. Gene expression analysis of Pax7 is represented in Figure 20 below.

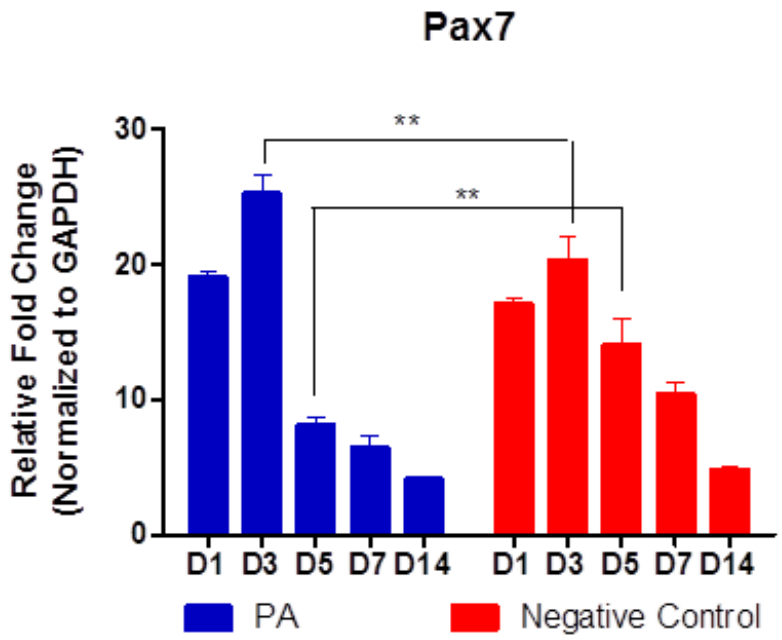

Figure 20 Pax7 gene expression analysis of skeletal muscle tissue in the rat model after PA or physiological saline treatment. Expression level of Pax7 gene was normalized against GAPDH. Error bars represent mean ± SEM, n=5 (***p<0.001, **p<0.01, *p<0.05)

The expression level of Pax7 gene was already high on day 1, but reached the highest level on day 3. This is a normal and expected result, because both quiescent and just-activated satellite cells express Pax7[69]. In addition, Pax-7 expressing myoblast cells are

heavily implicated in the regeneration of injured skeletal muscle fibers. Pax7 levels decreased after day 5 and no significant differences were observed between PA and control groups after this time period, which is also consistent with the previous literature, as myogenesis is well underway at this point and the increasing expression level of other myogenic factors (MyoD1 and Myf5) leads to the decrease of Pax7 gene expression. RT-qPCR results indicated that Pax7 expression was increased significantly in the LM/E-PA treated group on day 3. However, on day 5, Pax7 expression was significantly higher for the control group. By looking these data, it can be suggested that the myogenic regulatory changes experienced by the PA group on day 3 were only present in the control group at a later stage (day 5). This could be due to the early activation of satellite cells in the PA group through the stimulatory influence of the laminin-mimetic hydrogel environment. As a consequence of these striking results, Pax7 analysis gives us significant information about satellite cell activation during the first 14 days of myogenesis.

MyoD1 is a member of MRFs and takes a crucial part in the myogenesis process. The activation of MyoD1 occurs when skeletal muscle is damaged and mediates the satellite cell activation process in a series of cascade events. Gene expression analysis of MyoD1 is represented in Figure 21 below.

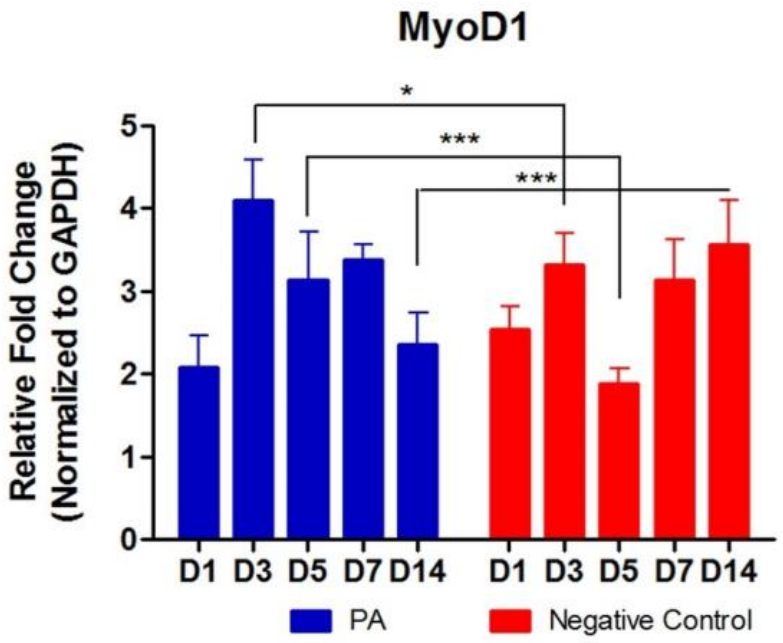

Figure 21 MyoD1 gene expression analysis of skeletal muscle tissue in the rat model after PA and physiological saline treatment. Expression level of MyoD1 gene was normalized against GAPDH. Error bars represent mean ± SEM, n=5 (***p<0.001, **p<0.01, *p<0.05)

Our results show that MyoD1 expression reached its highest level on day 3 in the PA treated group, at which point it was significantly higher than the control group. On the other hand, high expression levels for MyoD1 were observed on days 7 and 14 in the

control group. As with our Pax7 results, these observations suggest that the signaling networks involved in satellite cell activation were delayed in the control group compared to the PA-treated animals. This is expected, as satellite cell activation is facilitated by changes in Pax7 expression (which was also earlier in the PA group) and in return triggers an increase in the expression of MyoD1. Activated cells need to exit the cell cycle in order to differentiate, and it is known that MyoD1 has a role in cell cycle dismissal and stimulation of differentiation in myoblasts[70].

As noted above, our results also correspond closely with the Pax7 RT-qPCR data. Satellite cells are known to have different fates according to the expression balance between Pax7 and MyoD. Pax7+ / MyoD– cells return to quiescent satellite state while Pax7+ / MyoD+ cells are committed to myogenic differentiation[29]. Since Pax7 and MyoD expressions were observed at successive time points (one right after the other), it can be clearly said that satellite cells successfully committed to the myogenic differentiation. On the other hand, in the negative control group, higher MyoD1 expression on day 14 might be due to the slow activation of satellite cells. In conclusion, PA group exhibited accelerated satellite cell activation compared to the negative control group.

Myf5 is a transcription factor that is responsible for the activation of satellite cells during myogenesis and it is one of the earliest markers of differentiation. Gene expression analysis of Myf5 is represented in Figure 22 below.

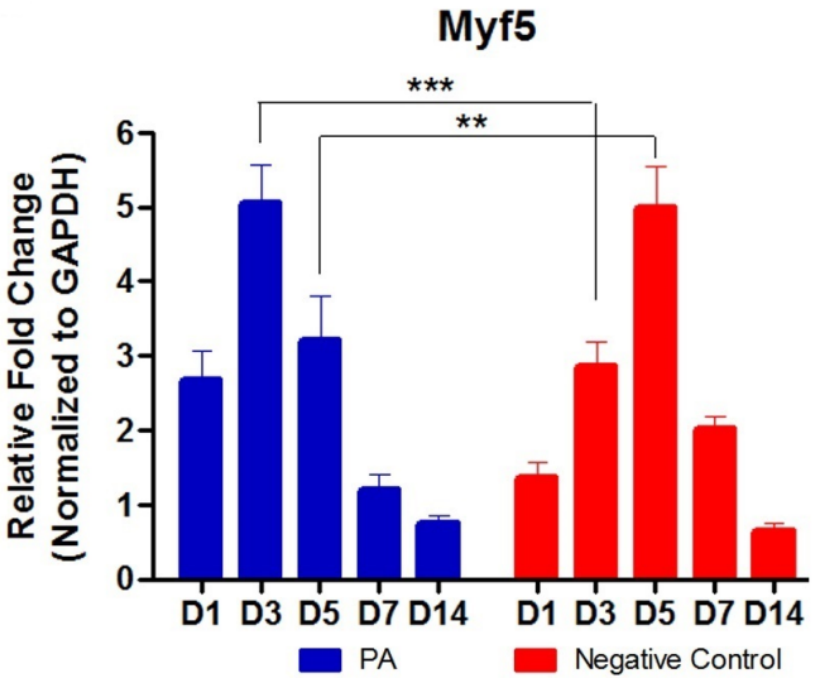

Figure 22 Myf5 gene expression analysis of skeletal muscle tissue in the rat model after PA or physiological saline treatment. Expression level of Myf5 gene was normalized against GAPDH. Error bars represent mean ± SEM, n=5 (***p<0.0001, **p<0.01, *p<0.05)

In present study, we showed that on day 3, Myf5 expression level was significantly higher in the PA group than the negative control group. Inversely, on day 5, Myf5 expression level was significantly lower in the PA group. The cause of this situation

might be the slow activation of satellite cells, because it is known that the balance between Pax7 and Myf5 controls the cell fate[27].

The combination of MyoD and Myf5 is also extremely necessary to skeletal muscle myogenesis[28]. As such, the present data suggest that Myf5-expressing cells were muscle progenitor cells, which exhibit a strong tendency to differentiate. We show that, in PA treated group, differentiation reached its highest level on day 3, but the same data was obtained on day 5 for the negative control group. This is very significant data and demonstrates that the PA treated group was more capable of activating differentiation markers at the molecular level.

Myogenin is another transcription factor and one of the latest markers of skeletal muscle regeneration. It is also essential for functional muscle formation. Gene expression analysis of Myogenin is represented in Figure 23 below.

High expression levels of myogenin were observed on day 7 and day 14, and the PA-treated group again exhibited higher expression levels compared to the physiological saline treated negative control group.

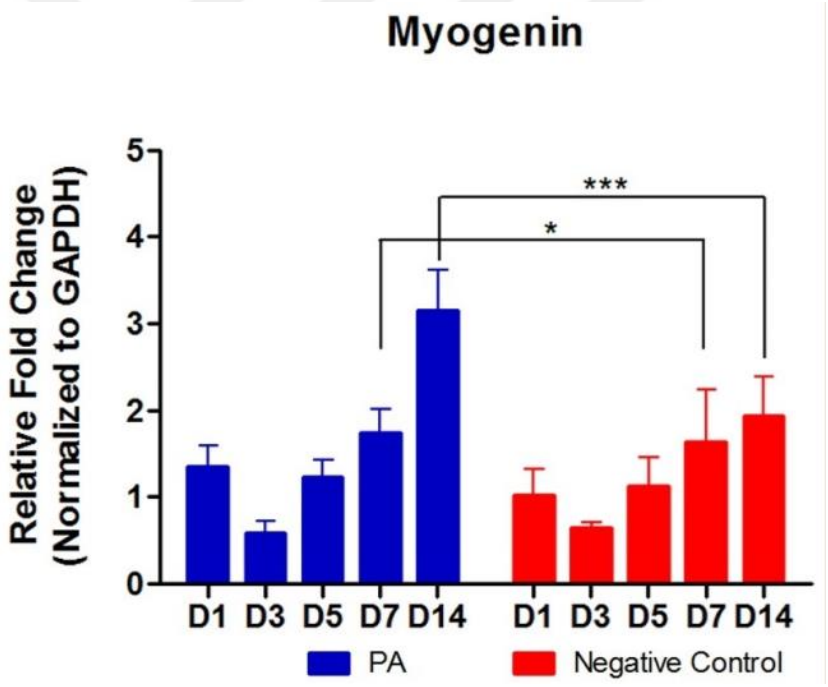

Figure 23 Myogenin gene expression analysis of skeletal muscle tissue in the rat model after PA or physiological saline treatment. Expression level of Myogenin gene was normalized against GAPDH. Error bars represent mean ± SEM, n=5 (***p<0.001, **p<0.01, *p<0.05)

Since myogenin is an indicator of freshly regenerated skeletal muscle fibers[30], we can say that our results are expected and accountable. The same myogenin expression patterns were observed in both PA and negative control groups. These data are also in agreement with the Pax7, MyoD1 and Myf5 data, suggesting skeletal muscle myogenesis occurs through the expression of overlapping markers (Figure 4). In conclusion, our findings support the idea that myogenesis is accelerated following the administration of laminin mimetic PA hydrogels, which actively interact with the satellite cells and facilitate their commitment to the myogenic lineage.

Overall, gene expression analyses, demonstrated that the activation of satellite cells and myogenic differentiation occurs at an earlier stage and to a greater extent in the presence of laminin mimetic peptide nanofibers, even without any additional treatment (growth factor addition etc.).

4.7 Protein Expression Analyses

Skeletal muscle myogenesis markers were detected and protein expression levels were quantified by Western blotting in early, middle and the late stages of myogenesis. The aim of checking these individual time points was to follow changes step by step during myogenesis. Four different myogenesis markers; Pax7, MyoD1, Myf5 and Myogenin (which were checked in real time PCR analysis) were used in western blot analysis as well. By checking these markers, we could also see the consistency between mRNA and protein expression. It is also possible to observe the effects of peptide hydrogels on the regeneration of skeletal muscle through Western blot analysis, as the protein expression profiles of myogenic transcription factors are strongly related with skeletal muscle regeneration.

Pax7 is one of the main transcription factors in satellite cells and its expression continues even after the initiation of their differentiation[68]. This makes Pax7 a good marker for the early steps of skeletal myogenesis, because both quiescent and just-activated satellite cells express this protein[69]. Pax-7 is also expressed by myoblast cells engaged in the regeneration of injured skeletal muscle fibers, and our immunoblotting results were consistent with the early activation of satellite cells in the laminin-mimetic bioactive scaffold (LM/E-PA) treated group (Figure 24).

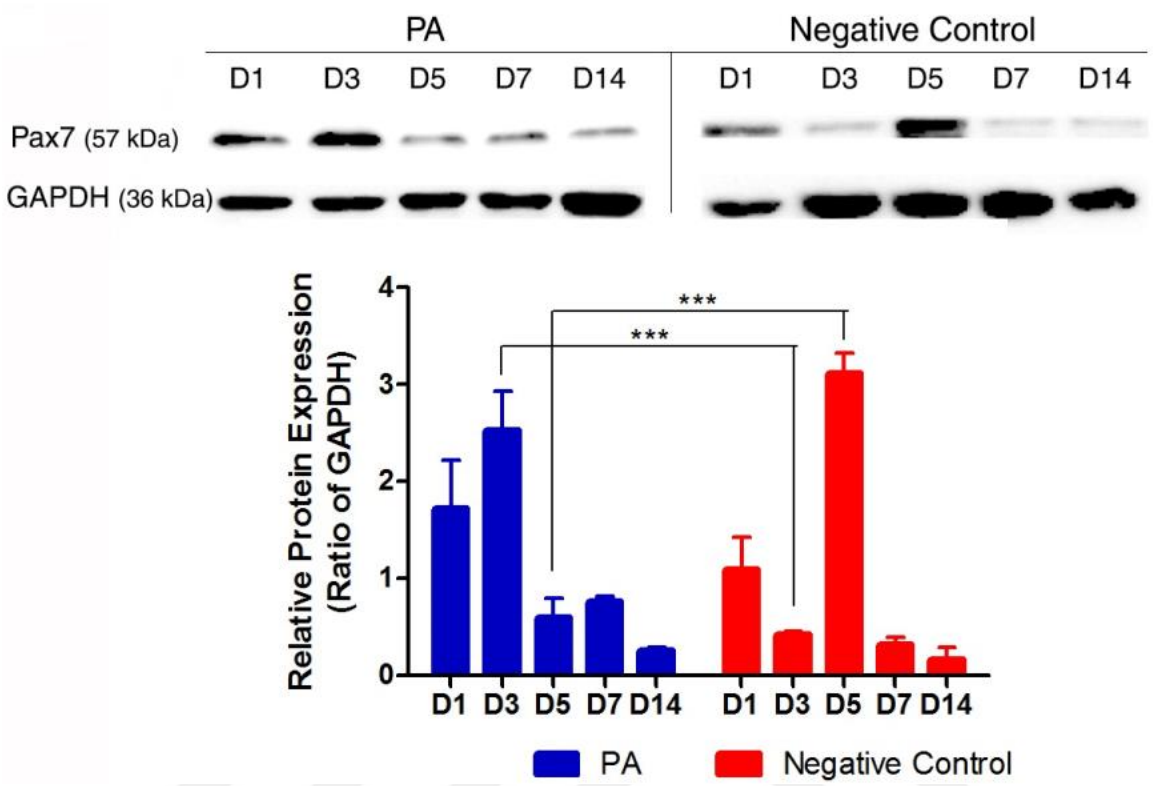

Figure 24 Western blots showing the expression and quantification of Pax7 protein in the myogenesis pathway in rat TA muscle lysates after cardiotoxin-induced muscle injury. Results were normalized to GAPDH and demonstrated for both PA and negative control groups. Error bars represent mean ± SEM, n=5 (***p<0.001, **p<0.01, *p<0.05)

The Pax7 findings were consistent with the RT-qPCR results. Early activation of satellite cells was observed in the bioactive PA treated group, leading to the initiation of myogenic differentiation.

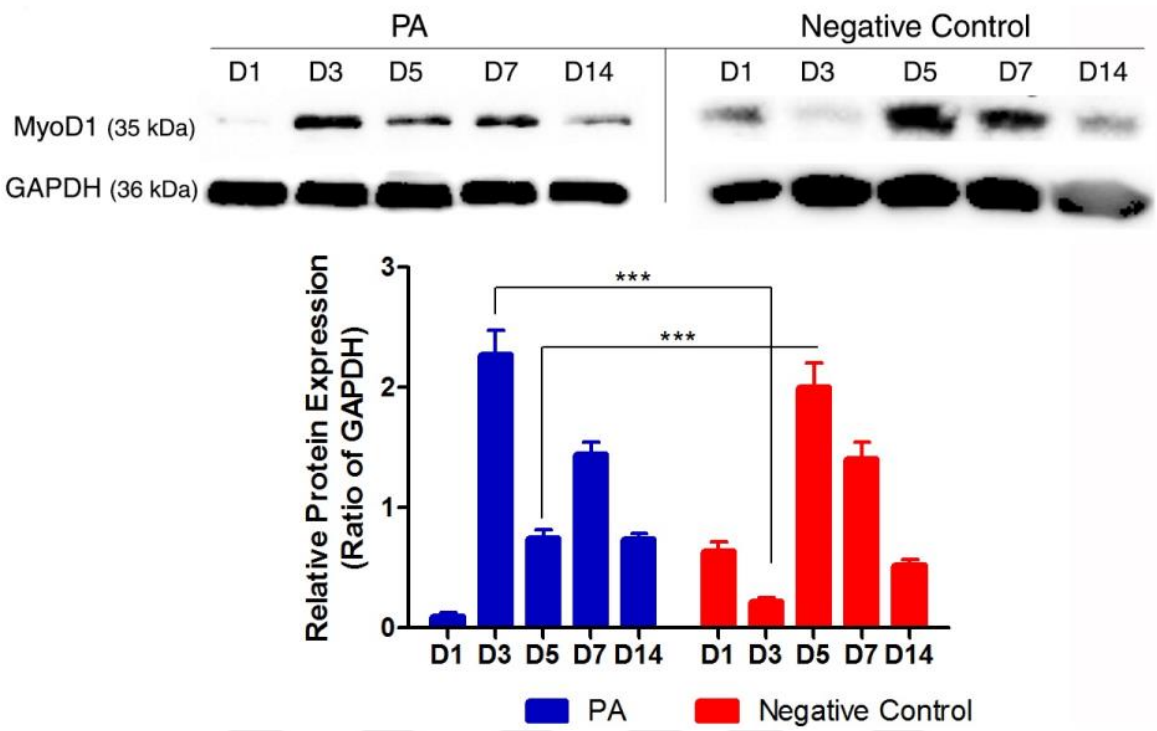

Figure 25 Western blots showing the expression and quantification of MyoD1 protein in the myogenesis pathway in rat TA muscle lysates after cardiotoxin-induced muscle injury. Results were normalized to GAPDH and demonstrated for both PA and negative control groups. Error bars represent mean ± SEM, n=5 (***p<0.001, **p<0.01, *p<0.05)

After day 5, it was observed that the increasing expression of other myogenic factors (MyoD1 and Myf5) led to the decrease of Pax7 gene expression (Figure 25). Activation of **MyoD1** is triggered when skeletal muscle is damaged, and results in a series of events that lead to satellite cell activation and, ultimately, skeletal muscle regeneration. Activated cells need to exit the cell cycle in order to differentiate (as mentioned above) and it is known that MyoD1 plays important roles in cell cycle dismissal and stimulation of differentiation in myoblasts. In addition, satellite cells have different fates according

to the expression balance between Pax7 and MyoD: Pax7+ / MyoD– cells return to quiescent satellite state while Pax7+ / MyoD+ cells are committed to myogenic differentiation[29]. As such, overall results are consistent with the Pax7 RT-qPCR and immunoblotting data, and suggest that satellite cell activation occurs at an earlier stage in the presence of the bioactive PA scaffold.

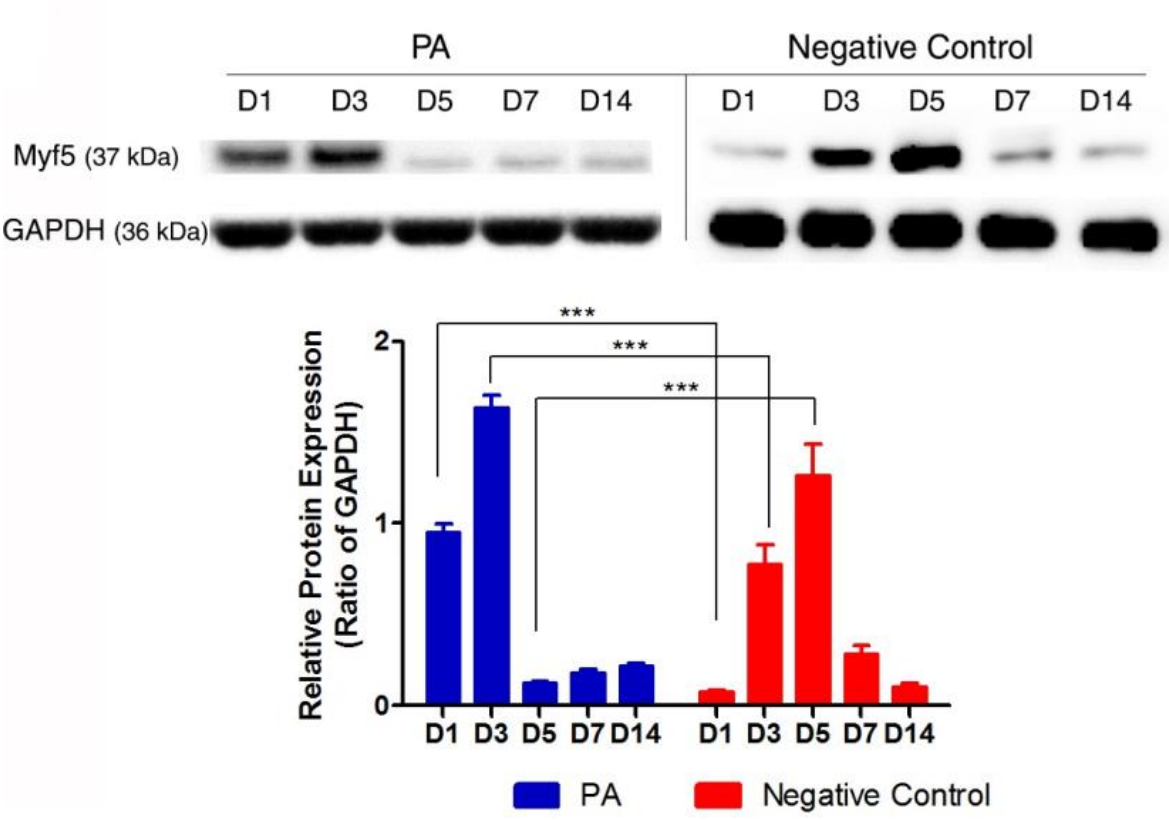

Figure 26 Western blots showing the expression and quantification of Myf5 protein in the myogenesis pathway in rat TA muscle lysates after cardiotoxin-induced muscle injury. Results were normalized to GAPDH and demonstrated for both PA and negative control groups. Error bars represent mean ± SEM, n=5 (***p<0.001, **p<0.01, *p<0.05)

Since Pax7 and MyoD1 expressions were observed at the same time points, it can be interpreted that satellite cells have successfully committed to myogenic differentiation. However, it is also known that the balance between Pax7 and Myf5 controls cell fate and that the combination of MyoD1 and Myf5 is extremely necessary for skeletal muscle myogenesis[27, 28]. As such, **Myf5**-expressing cells observed in the present study might be muscle progenitor cells, which have a high tendency to differentiate. We showed that differentiation reached its highest level on day 3 in the PA-treated group, while peak differentiation occured on day 5 for saline treatment (Figure 26). This result further confirms our initial data suggesting that laminin-mimetic PA scaffold treatment accelerates myogenic differentiation at the molecular level.

Myogenin is an indicator of freshly regenerated skeletal muscle fibers[30], and we have observed highest myogenin expression on day 14. Western blot analysis of Myogenin is represented in Figure 27 below.

This data also agrees with the Pax7, MyoD1 and Myf5 data for both RT-qPCR and immunoblotting results, suggesting that skeletal muscle myogenesis occurs through overlapping expression of markers.

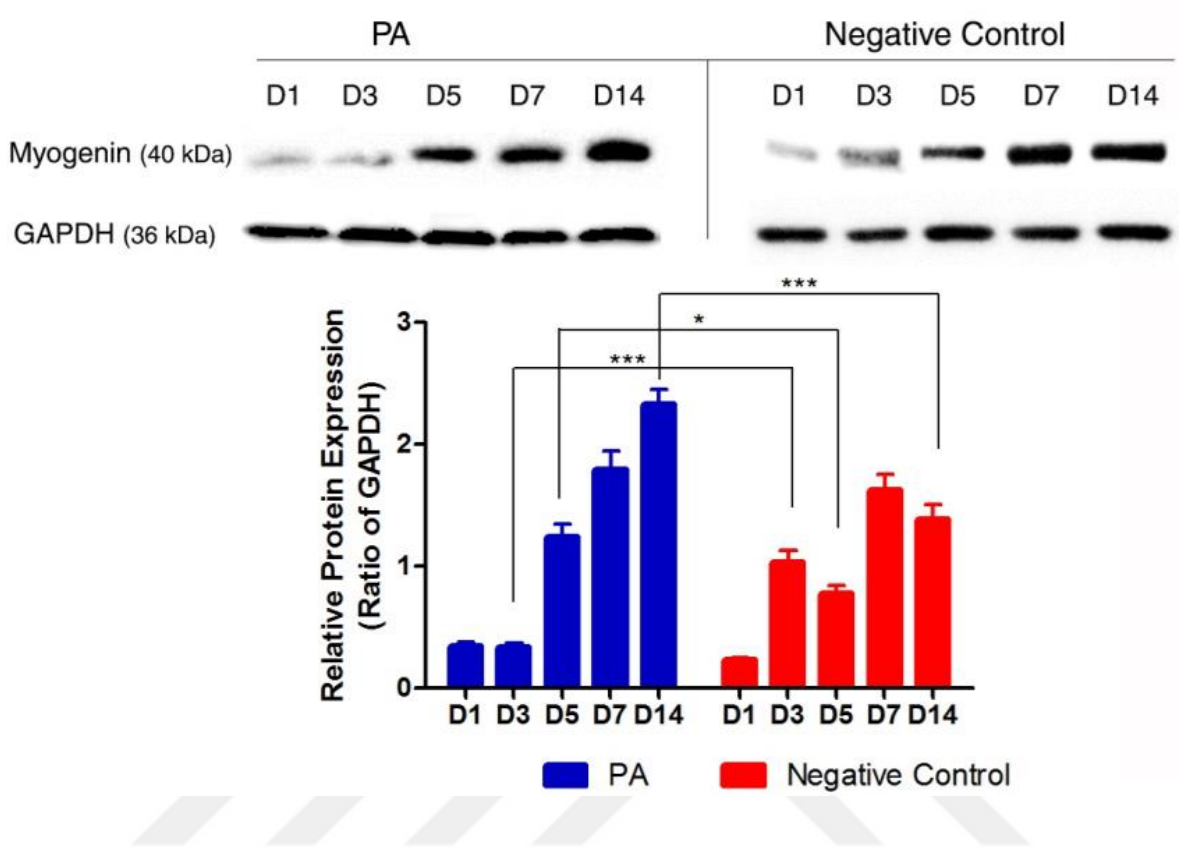

Figure 27 Western blots showing the expression and quantification of Myogenin protein in the myogenesis pathway in rat TA muscle lysates after cardiotoxin-induced muscle injury. Results were normalized to GAPDH and demonstrated for both PA and negative control groups. Error bars represent mean ± SEM, n=5 (***p<0.001, **p<0.01, *p<0.05)

Our findings support the idea that myogenesis is accelerated at the molecular level in the presence of laminin mimetic bioactive scaffolds that can interact with satellite cells and facilitate their commitment to the myogenic lineage. Present gene expression and protein detection analyses demonstrated that the activation of satellite cells and myogenic differentiation occurs at an earlier stage and to a greater extent on laminin-mimetic peptide nanofibers, even without any additional treatment.

5 Conclusion

Skeletal muscle injury is one of the most frequently encountered problems among people, especially athletes and elders. Body posture is based on skeletal muscle organization; as such, it is directly related with the quality of life. Even bodybuilders are in search of faster and effective skeletal muscle regeneration tips for better physical appearance. Both quality of life and physical attractiveness are directly linked with our skeletal muscle tissue.

The complete regeneration of skeletal muscle can only be achieved if an adequate number of satellite cells undergo myogenic differentiation and are induced to trigger the regeneration process through molecular-level signals. The main problem related with skeletal muscle injuries is the low number of activated satellite cells merging with muscle fibers and the lack of bioactive signals controlling molecular-level myogenesis. That is why, in many cases, low and ineffective regeneration is present and fibrous tissue is produced instead of muscular tissue during skeletal muscle regeneration.

Rapid and effective muscle regeneration may be possible if we have a better understanding about the molecular events behind skeletal muscle regeneration and myogenic differentiation. In particular, new tissue formation can be effectively facilitated with the help of successfully mimicking microenvironment production.

The present thesis has revealed the inductive role of a laminin-mimetic bioactive scaffold (LM/E-PA) for new skeletal muscle tissue formation via myogenic differentiation of progenitor satellite cells *in vivo*. In skeletal muscle, the basal lamina is responsible for mediating a broad range of regulatory signals between satellite cells and

their environment. Mimicking such a microenvironment is important for regulating myoblast differentiation. If skeletal muscle progenitor cells are able to interact with our scaffold system in ways similar to their interactions with their native ECM, they would be strongly encouraged to differentiate from myoblasts to myofibers. Our results suggest that this condition is satisfied and that we are able to provide an ECM-like microenvironment by using laminin-mimetic nanofibers for progenitor cells following acute muscle injury.

In this thesis, we first performed a review of *in vitro* study results that were conducted in our lab before. Since laminin is one of the most abundant basal membrane proteins of skeletal muscle tissue, a laminin-mimetic bioactive scaffold system was chosen as a model to study myogenic differentiation. According to a previous study, myogenic differentiation of C2C12 cells is enhanced in the presence of the laminin mimetic bioactive scaffold (LM/E-PA) system. However, *in vivo* tests are necessary to fully establish the effectiveness of this system for therapeutic purposes. As such, we sought to use this system in a rat muscle injury model to determine whether it would be suitable for further research and modification. Acute muscle injuries were created in the TA muscles and the LM/E-PA scaffold system was injected to evaluate its regenerative effect on severe muscle injuries. In addition, physiological saline was injected to the opposite legs of treated animals as a negative control. Our EMG and step test observations suggest that the scaffold system is supportive of physical and functional recovery. Molecular level gene expression and protein detection analyses also supported the idea that LM/E-PA scaffold system provides faster regeneration through the early initiation of myogenic differentiation of satellite cells *in vivo*.

In conclusion, the laminin-derived IKVAV scaffold system promoted satellite cell activation and myogenic differentiation *in vivo*. Since laminin is a major component of the basal lamina of skeletal muscle tissue, LM/E-PA treatment accelerated skeletal muscle regeneration by enhanced satellite cell recruitment and muscle fiber enlargement. Together, our findings underline the ability of the laminin-mimetic bioactive scaffold to enhance the regeneration of acute muscle injuries through its interactions with molecular cascades involved in muscle repair. This is the first study to demonstrate the stimulation of myogenesis and muscle regeneration with laminin-mimetic bioactive nanofiber scaffolds *in vivo*. Due to its mimicry of extracellular matrix and ease of application by injection, the laminin mimetic bioactive scaffold is a promising material for promoting skeletal muscle regeneration for future clinical applications.

6 Future Perspectives

Skeletal muscle is a tissue that is constantly exposed to external mechanical influences, which greatly complicates its therapy and protection. Therefore, complete and effective regeneration of skeletal muscle is very challenging. Mechanical options might be incorporated into the design of bioactive scaffold systems to further enhance their effectiveness. For future studies, it is essential to use higher level organisms to improve our current findings and treatment options for skeletal muscle regeneration. More extensive molecular level analysis, such as that pertaining to pathways regulating myogenic differentiation, might be performed to determine the exact mechanism of action of the laminin-mimetic scaffolds. In order to develop drugs as a furthest step, collaborations might be done with the pharmaceutical companies.

BIBLIOGRAPHY

1. Mackey, A. L.; Kjaer, M., Connective tissue regeneration in skeletal muscle after eccentric contraction-induced injury. *J Appl Physiol (1985)* **2016**, jap.00577.2016.

2. McCall, G. E.; Byrnes, W. C.; Dickinson, A.; Pattany, P. M.; Fleck, S. J., Muscle fiber hypertrophy, hyperplasia, and capillary density in college men after resistance training. *J Appl Physiol (1985)* **1996,** *81* (5), 2004-12.

3. Moritani, T.; deVries, H. A., Neural factors versus hypertrophy in the time course of muscle strength gain. *Am J Phys Med* **1979,** *58* (3), 115-30.

4. Ekstrand, J.; Hägglund, M.; Waldén, M., Epidemiology of muscle injuries in professional football (soccer). *Am J Sports Med* **2011,** *39* (6), 1226-32.

5. Chan, O.; Del Buono, A.; Best, T. M.; Maffulli, N., Acute muscle strain injuries: a proposed new classification system. *Knee Surg Sports Traumatol Arthrosc* **2012,** *20* (11), 2356-62.

6. Juhas, M.; Bursac, N., Engineering skeletal muscle repair. *Curr Opin Biotechnol* **2013,** *24* (5), 880-6.

7. Järvinen, T. A.; Järvinen, T. L.; Kääriäinen, M.; Kalimo, H.; Järvinen, M., Muscle injuries: biology and treatment. *Am J Sports Med* **2005,** *33* (5), 745-64.

8. Ricotti, L.; Polini, A.; Genchi, G. G.; Ciofani, G.; Iandolo, D.; Vazão, H.; Mattoli, V.; Ferreira, L.; Menciassi, A.; Pisignano, D., Proliferation and skeletal myotube formation capability of C2C12 and H9c2 cells on isotropic and anisotropic electrospun nanofibrous PHB scaffolds. *Biomed Mater* **2012,** *7* (3), 035010.

9. Cerletti, M.; Jurga, S.; Witczak, C. A.; Hirshman, M. F.; Shadrach, J. L.; Goodyear, L. J.; Wagers, A. J., Highly efficient, functional engraftment of skeletal muscle stem cells in dystrophic muscles. *Cell* **2008,** *134* (1), 37-47.

10. Maffulli, N.; Del Buono, A.; Oliva, F.; Giai Via, A.; Frizziero, A.; Barazzuol, M.; Brancaccio, P.; Freschi, M.; Galletti, S.; Lisitano, G.; Melegati, G.; Nanni, G.; Pasta, G.; Ramponi, C.; Rizzo, D.; Testa, V.; Valent, A., Muscle Injuries: A Brief Guide to Classification and Management. *Transl Med UniSa* **2015,** *12*, 14-8.

11. Zhang, Q. Z., Dystroglycan induced muscular dystrophies - a review. *Eur Rev Med Pharmacol Sci* **2016,** *20* (17), 3683-7.

12. Tsitkanou, S.; Spengos, K.; Stasinaki, A. N.; Zaras, N.; Bogdanis, G.; Papadimas, G.; Terzis, G., Effects of high-intensity interval cycling performed after resistance training on muscle strength and hypertrophy. *Scand J Med Sci Sports* **2016**.

13. Gigliotti, D.; Leiter, J. R.; MacDonald, P. B.; Peeler, J.; Anderson, J. E., Altered Satellite Cell Responsiveness and Denervation Implicated in Progression of Rotator-Cuff Injury. *PLoS One* **2016,** *11* (9), e0162494.

14. Han, W. M.; Jang, Y. C.; García, A. J., Engineered matrices for skeletal muscle satellite cell engraftment and function. *Matrix Biol* **2016**.

15. Gurevich, D. B.; Nguyen, P. D.; Siegel, A. L.; Ehrlich, O. V.; Sonntag, C.; Phan, J. M.; Berger, S.; Ratnayake, D.; Hersey, L.; Berger, J.; Verkade, H.; Hall, T. E.; Currie, P. D., Asymmetric division of clonal muscle stem cells coordinates muscle regeneration in vivo. *Science* **2016,** *353* (6295), aad9969.

16. Scime, A.; Caron, A. Z.; Grenier, G., Advances in myogenic cell transplantation and skeletal muscle tissue engineering. *Front Biosci (Landmark Ed)* **2009,** *14*, 3012-23.

17. Gillies, A. R.; Lieber, R. L., Structure and function of the skeletal muscle extracellular matrix. *Muscle Nerve* **2011,** *44* (3), 318-31.

18. Carpenter, S.; Karpati, G., Segmental necrosis and its demarcation in experimental micropuncture injury of skeletal muscle fibers. *J Neuropathol Exp Neurol* **1989,** *48* (2), 154-70.

19. Frenette, J.; Cai, B.; Tidball, J. G., Complement activation promotes muscle inflammation during modified muscle use. *Am J Pathol* **2000,** *156* (6), 2103-10.

20. Huard, J.; Li, Y.; Fu, F. H., Muscle injuries and repair: current trends in research. *J Bone Joint Surg Am* **2002,** *84-A* (5), 822-32.

21. Zammit, P.; Beauchamp, J., The skeletal muscle satellite cell: stem cell or son of stem cell? *Differentiation* **2001,** *68* (4-5), 193-204.

22. Sheehan, S. M.; Allen, R. E., Skeletal muscle satellite cell proliferation in response to members of the fibroblast growth factor family and hepatocyte growth factor. *J Cell Physiol* **1999,** *181* (3), 499-506.

23. Olfert, I. M.; Howlett, R. A.; Wagner, P. D.; Breen, E. C., Myocyte vascular endothelial growth factor is required for exercise-induced skeletal muscle angiogenesis. *Am J Physiol Regul Integr Comp Physiol* **2010,** *299* (4), R1059-67.

24. Järvinen, T. A.; Järvinen, M.; Kalimo, H., Regeneration of injured skeletal muscle after the injury. *Muscles Ligaments Tendons J* **2013,** *3* (4), 337-45.

25. Bergstrom, D. A.; Tapscott, S. J., Molecular distinction between specification and differentiation in the myogenic basic helix-loop-helix transcription factor family. *Mol Cell Biol* **2001,** *21* (7), 2404-12.

26. Motohashi, N.; Asakura, A., Muscle satellite cell heterogeneity and self-renewal. *Front Cell Dev Biol* **2014,** *2*, 1.

27. Kuang, S.; Kuroda, K.; Le Grand, F.; Rudnicki, M. A., Asymmetric self-renewal and commitment of satellite stem cells in muscle. *Cell* **2007,** *129* (5), 999-1010.

28. Rudnicki, M. A.; Schnegelsberg, P. N.; Stead, R. H.; Braun, T.; Arnold, H. H.; Jaenisch, R., MyoD or Myf-5 is required for the formation of skeletal muscle. *Cell* **1993,** *75* (7), 1351-9.

29. Zammit, P. S.; Golding, J. P.; Nagata, Y.; Hudon, V.; Partridge, T. A.; Beauchamp, J. R., Muscle satellite cells adopt divergent fates: a mechanism for self-renewal? *J Cell Biol* **2004,** *166* (3), 347-57.

30. Yan, Z.; Choi, S.; Liu, X.; Zhang, M.; Schageman, J. J.; Lee, S. Y.; Hart, R.; Lin, L.; Thurmond, F. A.; Williams, R. S., Highly coordinated gene regulation in mouse skeletal muscle regeneration. *J Biol Chem* **2003,** *278* (10), 8826-36.

31. Lieber, R. L.; Steinman, S.; Barash, I. A.; Chambers, H., Structural and functional changes in spastic skeletal muscle. *Muscle Nerve* **2004,** *29* (5), 615-27.

32. Wu, M. C.; Forbes, J. G.; Wang, K., Disorder profile of nebulin encodes a vernierlike position sensor for the sliding thin and thick filaments of the skeletal muscle sarcomere. *Phys Rev E* **2016,** *93* (6), 062406.

33. Burghardt, T. P.; Sun, X.; Wang, Y.; Ajtai, K., In vitro and in vivo single myosin step-sizes in striated muscle. *J Muscle Res Cell Motil* **2015,** *36* (6), 463-77.

34. Takeda, S.; Yamashita, A.; Maeda, K.; Maéda, Y., Structure of the core domain of human cardiac troponin in the Ca(2+)-saturated form. *Nature* **2003,** *424* (6944), 35-41.

35. Gunning, P. W.; Schevzov, G.; Kee, A. J.; Hardeman, E. C., Tropomyosin isoforms: divining rods for actin cytoskeleton function. *Trends Cell Biol* **2005,** *15* (6), 333-41.

36. Labeit, S.; Kolmerer, B., Titins: giant proteins in charge of muscle ultrastructure and elasticity. *Science* **1995,** *270* (5234), 293-6.

37. Frantz, C.; Stewart, K. M.; Weaver, V. M., The extracellular matrix at a glance. *J Cell Sci* **2010,** *123* (Pt 24), 4195-200.

38. Rozario, T.; DeSimone, D. W., The extracellular matrix in development and morphogenesis: a dynamic view. *Dev Biol* **2010,** *341* (1), 126-40.

39. Anderson, C.; Winder, S. J.; Borycki, A. G., Dystroglycan protein distribution coincides with basement membranes and muscle differentiation during mouse embryogenesis. *Dev Dyn* **2007,** *236* (9), 2627-35.

40. Fraser, R. D.; MacRae, T. P.; Miller, A., Molecular packing in type I collagen fibrils. *J Mol Biol* **1987,** *193* (1), 115-25.

41. Colognato, H.; Yurchenco, P. D., Form and function: the laminin family of heterotrimers. *Dev Dyn* **2000,** *218* (2), 213-34.

42. Ervasti, J. M.; Campbell, K. P., A role for the dystrophin-glycoprotein complex as a transmembrane linker between laminin and actin. *J Cell Biol* **1993,** *122* (4), 809-23.

43. Gawlik, K. I.; Durbeej, M., Skeletal muscle laminin and MDC1A: pathogenesis and treatment strategies. *Skelet Muscle* **2011,** *1* (1), 9.

44. Foster, R. F.; Thompson, J. M.; Kaufman, S. J., A laminin substrate promotes myogenesis in rat skeletal muscle cultures: analysis of replication and development using antidesmin and anti-BrdUrd monoclonal antibodies. *Dev Biol* **1987,** *122* (1), 11-20.

45. Sanes, J. R., The basement membrane/basal lamina of skeletal muscle. *J Biol Chem* **2003,** *278* (15), 12601-4.

46. Tashiro, K.; Sephel, G. C.; Weeks, B.; Sasaki, M.; Martin, G. R.; Kleinman, H. K.; Yamada, Y., A synthetic peptide containing the IKVAV sequence from the A chain of laminin mediates cell attachment, migration, and neurite outgrowth. *J Biol Chem* **1989,** *264* (27), 16174-82.

47. Fuoco, C.; Rizzi, R.; Biondo, A.; Longa, E.; Mascaro, A.; Shapira-Schweitzer, K.; Kossovar, O.; Benedetti, S.; Salvatori, M. L.; Santoleri, S.; Testa, S.; Bernardini, S.; Bottinelli, R.; Bearzi, C.; Cannata, S. M.; Seliktar, D.; Cossu, G.; Gargioli, C., In vivo generation of a mature and functional artificial skeletal muscle. *EMBO Mol Med* **2015,** *7* (4), 411-22.

48. Baoge, L.; Van Den Steen, E.; Rimbaut, S.; Philips, N.; Witvrouw, E.; Almqvist, K. F.; Vanderstraeten, G.; Vanden Bossche, L. C., Treatment of skeletal muscle injury: a review. *ISRN Orthop* **2012,** *2012*, 689012.

49. Chan, Y. S.; Li, Y.; Foster, W.; Fu, F. H.; Huard, J., The use of suramin, an antifibrotic agent, to improve muscle recovery after strain injury. *Am J Sports Med* **2005,** *33* (1), 43-51.

50. Lodi, R.; Hart, P. E.; Rajagopalan, B.; Taylor, D. J.; Crilley, J. G.; Bradley, J. L.; Blamire, A. M.; Manners, D.; Styles, P.; Schapira, A. H.; Cooper, J. M., Antioxidant treatment improves in vivo cardiac and skeletal muscle bioenergetics in patients with Friedreich's ataxia. *Ann Neurol* **2001,** *49* (5), 590-6.

51. Fuoco, C.; Petrilli, L. L.; Cannata, S.; Gargioli, C., Matrix scaffolding for stem cell guidance toward skeletal muscle tissue engineering. *J Orthop Surg Res* **2016,** *11* (1), 86.

52. Hartgerink, J. D.; Beniash, E.; Stupp, S. I., Peptide-amphiphile nanofibers: a versatile scaffold for the preparation of self-assembling materials. *Proc Natl Acad Sci U S A* **2002,** *99* (8), 5133-8.

53. Newcomb, C. J.; Sur, S.; Ortony, J. H.; Lee, O. S.; Matson, J. B.; Boekhoven, J.; Yu, J. M.; Schatz, G. C.; Stupp, S. I., Cell death versus cell survival instructed by supramolecular cohesion of nanostructures. *Nat Commun* **2014,** *5*, 3321.

54. Mammadov, R.; Mammadov, B.; Toksoz, S.; Aydin, B.; Yagci, R.; Tekinay, A. B.; Guler, M. O., Heparin mimetic peptide nanofibers promote angiogenesis. *Biomacromolecules* **2011,** *12* (10), 3508-19.

55. Arslan, E.; Garip, I. C.; Gulseren, G.; Tekinay, A. B.; Guler, M. O., Bioactive supramolecular peptide nanofibers for regenerative medicine. *Adv Healthc Mater* **2014,** *3* (9), 1357-76.

56. Yasa, I. C.; Gunduz, N.; Kilinc, M.; Guler, M. O.; Tekinay, A. B., Basal Lamina Mimetic Nanofibrous Peptide Networks for Skeletal Myogenesis. *Sci Rep* **2015,** *5*, 16460.

57. MERRIFIELD, R. B., SOLID-PHASE PEPTIDE SYNTHESES. *Endeavour* **1965,** *24*, 3-7.

58. Fernagut, P. O.; Diguet, E.; Labattu, B.; Tison, F., A simple method to measure stride length as an index of nigrostriatal dysfunction in mice. *J Neurosci Methods* **2002,** *113* (2), 123-30.

59. Paramonov, S. E.; Jun, H. W.; Hartgerink, J. D., Self-assembly of peptide-amphiphile nanofibers: the roles of hydrogen bonding and amphiphilic packing. *J Am Chem Soc* **2006,** *128* (22), 7291-8.

60. Cui, H.; Webber, M. J.; Stupp, S. I., Self-assembly of peptide amphiphiles: from molecules to nanostructures to biomaterials. *Biopolymers* **2010,** *94* (1), 1-18.

61. Souron, R.; Farabet, A.; Féasson, L.; Belli, A.; Millet, G. Y.; Lapole, T., Effects of an 8-week local vibration training on corticospinal properties of the tibialis anterior muscle. *Ann Phys Rehabil Med* **2016,** *59S*, e52.

62. Salomone, R.; Costa, H. J.; Rodrigues, J. R.; Reis e Silva, S. M.; Ovando, P. C.; Orando, P. C.; Bento, R. F., Assessment of a neurophysiological model of the mandibular branch of the facial nerve in rats by electromyography. *Ann Otol Rhinol Laryngol* **2012,** *121* (3), 179-84.

63. Ilha, J.; Araujo, R. T.; Malysz, T.; Hermel, E. E.; Rigon, P.; Xavier, L. L.; Achaval, M., Endurance and resistance exercise training programs elicit specific effects on sciatic nerve regeneration after experimental traumatic lesion in rats. *Neurorehabil Neural Repair* **2008,** *22* (4), 355-66.

64. Nepomuceno, A. C.; Politani, E. L.; Silva, E. G.; Salomone, R.; Longo, M. V.; Salles, A. G.; Faria, J. C.; Gemperli, R., Tibial and fibular nerves evaluation using intraoperative electromyography in rats. *Acta Cir Bras* **2016,** *31* (8), 542-8.

65. Ostrovidov, S.; Shi, X.; Sadeghian, R. B.; Salehi, S.; Fujie, T.; Bae, H.; Ramalingam, M.; Khademhosseini, A., Stem Cell Differentiation Toward the Myogenic Lineage for Muscle Tissue Regeneration: A Focus on Muscular Dystrophy. *Stem Cell Rev* **2015,** *11* (6), 866-84.

66. Schantz, P.; Randall-Fox, E.; Hutchison, W.; Tydén, A.; Astrand, P. O., Muscle fibre type distribution, muscle cross-sectional area and maximal voluntary strength in humans. *Acta Physiol Scand* **1983,** *117* (2), 219-26.

67. Folker, E. S.; Baylies, M. K., Nuclear positioning in muscle development and disease. *Front Physiol* **2013,** *4*, 363.

68. Reimann, J.; Brimah, K.; Schröder, R.; Wernig, A.; Beauchamp, J. R.; Partridge, T. A., Pax7 distribution in human skeletal muscle biopsies and myogenic tissue cultures. *Cell Tissue Res* **2004,** *315* (2), 233-42.

69. Seale, P.; Sabourin, L. A.; Girgis-Gabardo, A.; Mansouri, A.; Gruss, P.; Rudnicki, M. A., Pax7 is required for the specification of myogenic satellite cells. *Cell* **2000,** *102* (6), 777-86.

70. Kitzmann, M.; Carnac, G.; Vandromme, M.; Primig, M.; Lamb, N. J.; Fernandez, A., The muscle regulatory factors MyoD and myf-5 undergo distinct cell cycle-specific expression in muscle cells. *J Cell Biol* **1998,** *142* (6), 1447-59.